Chapter 10 in the book:
P.A. Kralchevsky and K. Nagayama, "Particles at Fluid Interfaces and Membranes"
(Attachment of Colloid Particles and Proteins to Interfaces and Formation of Two-Dimensional Arrays)
Elsevier, Amsterdam, 2001; pp. 426-468.

CHAPTER 10

MECHANICS OF LIPID MEMBRANES AND INTERACTION BETWEEN INCLUSIONS

A bilayer lipid membrane cannot be simply modeled as a thin liquid film because the hydrocarbon-chain interior of the membrane exhibits elastic behavior when its thickness is varied. The hybrid mechanical behavior of a lipid bilayer (neither liquid nor bulk elastic body) can be described by means of a mechanical model, which treats the membrane as a special elastic film (the hydrocarbon chain interior) sandwiched between two Gibbs dividing surfaces (the surface polar-headgroup layers of the membrane). The latter *"sandwich" model* involves mechanical parameters such as the shear elastic modulus of the hydrocarbon chain interior, the bilayer surface tension, stretching (Gibbs) elasticity, surface bending moment and curvature elastic moduli. A mechanical analysis of the bilayer deformations enables one to derive expressions for the total stretching, bending and torsion (Gaussian) moduli of the membrane as a whole in terms of the aforementioned mechanical parameters of the model.

Inclusions in a lipid membrane (like membrane proteins) cause deformations in the bilayer surfaces accompanied by displacements in the membrane hydrocarbon interior. The presented mechanical model provides a set of differential equations, which could have both monotonic and oscillatory solutions for the membrane profile. In the case of not-too-low membrane surface tension the shape of the membrane surfaces is governed by an analogue of the Laplace equation of capillarity. The theory of the lateral capillary forces, presented in Chapter 7, is extended and applied to describe the interactions between two inclusions in a lipid membrane. The range of the obtained attractive force turns out to be of the order of several inclusion radii. The magnitude of interaction is estimated to be sufficient to bring about aggregation of the inclusions. The theoretical predictions are consonant with the experimental observations, although more reliable data about the membrane mechanical parameters are needed to achieve an actually quantitative comparison. The presented mechanical model of lipid membranes can be helpful for the theoretical description and interpretation of various processes involving bilayer deformations and interactions between protein inclusions.

10.1. DEFORMATIONS IN A LIPID MEMBRANE DUE TO THE PRESENCE OF INCLUSIONS

The integral (transmembrane) proteins, having a relatively rigid structure, create some deformations in the surrounding lipid membrane (Fig. 10.1). The overlap of such two deformed zones is expected to give rise to a membrane (lipid) mediated protein-protein interaction, as it is for particles confined into a liquid film (Chapter 7) or floating on a liquid interface (Chapter 8). Actually, the experiment shows that some integral proteins can form two-dimensional ordered arrays in native membranes [1-6], which can be attributed to interactions of this kind. Although the physical basis of the interactions between inclusions in liquid films and in lipid membranes is similar (overlap of deformations), the formalism developed in Chapters 7 and 8 for liquid interfaces and films cannot be *directly* applied to the case of lipid membranes, because of their more complicated mechanical properties. Some elastic properties of the membrane interior and surfaces should be taken into account to develop an adequate mechanical model of a lipid bilayer. For review on membrane properties see Refs. [6-8].

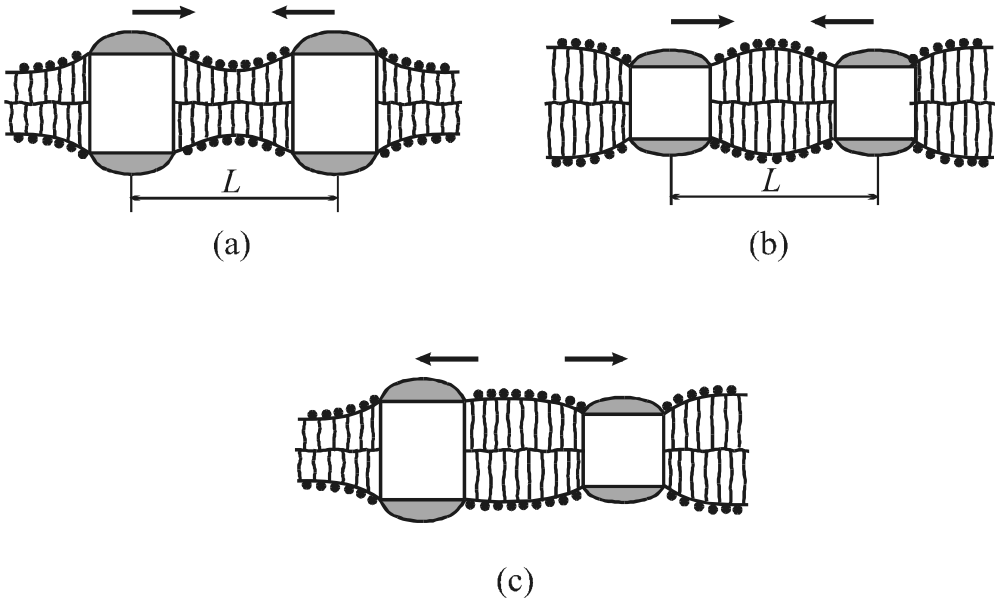

Fig. 10.1. The hydrophobic thickness of an inclusion (transmembrane protein) can be (a) greater or (b) smaller than the thickness of the non-disturbed phospholipid bilayer. The overlap of the deformations around two similar inclusions gives rise to attraction between them. In the case of dissimilar inclusions (c) repulsion is expected.

A variety of theoretical models have been proposed to describe the properties of phospholipid bilayers [9-18]. Generally, two types of models can be distinguished. The first type includes *molecular* models explicitly accounting for the lipid-lipid interactions (of van der Waals, electrostatic and steric origin) as well as for the configurational entropy of the hydrocarbon chains [11,13]. Similar are the mean-field models based on calculation of the energy and entropy of a given lipid molecule by averaging over all possible chain configurations of its neighbors [9,10,12]. These models give predictions about the elastic constants, spontaneous curvature, chain order parameter, etc. Two essential conclusions can be drawn from these studies: (i) the CH_2-group density and ordering are rather uniform across the membrane [10,12,13] and (ii) the lipid hydrocarbon tails strongly interact with each other and create significant mechanical stresses in the membrane interior.

The second type of *phenomenological* models [11,14-18] allows one to calculate the variation of the membrane shape, energy, etc., around a given non-perturbed state using some phenomenological relationships and parameters, such as interfacial tension, stretching and bending elastic moduli, spontaneous curvature of the constituent lipid monolayers, elasticity of the hydrocarbon core, and others.

An approach to the lipid-mediated interactions between the membrane proteins, based on the calculation of the chain interaction energy and entropy, has been developed in several works [9,19-21]. This theoretical approach is related to the experimental findings that proteins incorporated in membranes perturb the neighboring lipid molecules [22-24], and especially affect the fluidity of their hydrocarbon chains. However, experiments performed by means of ESR and NMR methods demonstrated that the degree of ordering and fluidity of the hydrocarbon chains of lipid molecules bound to membrane proteins is not very different from those of unbound molecules [25-27], in contract with the initial hypotheses [9,19].

Other idea about the origin of the membrane-mediated interactions between inclusions stems from the experiments by Chen and Hubbell [28], who have observed aggregation of the transmembrane protein rhodopsin in cases in which there has been a *mismatch* between the width of the hydrophobic belt of the protein and the thickness of the hydrophobic interior of the lipid bilayer, see Fig. 10.1b. These results imply that the perturbation of the bilayer thickness in

a vicinity of an incorporated protein may give rise to protein-protein attraction. This effect was studied both experimentally [29-34] and theoretically [35-41]; see Ref. [6] for a recent review. Lewis and Engelman [30] showed that bacteriorhodopsin forms aggregates in the membrane of vesicles (prepared from lipids of different chain length) only when the mismatch is greater than 1 nm for thinner bilayers (Fig. 10.1a) and 0.4 nm for thicker bilayers (Fig. 10.1b). Likewise, protein aggregation at considerable hydrophobic mismatch was detected with other natural proteins [29,31,32,34] and synthesized polypeptides [31]. As noted above, if two different protein inclusions create mismatches of the opposite sign, see Fig. 10.1c, then repulsion between the inclusions is expected [42].

Dan et al. [38] proposed a relatively simple phenomenological description, which models a lipid bilayer as two identical tensionless surfaces separated at a distance equal to the local bilayer hydrophobic thickness; see also Refs. [39-41]. Each of these surfaces models a tensionless monolayer, which possesses its own bending elasticity (stiffness) and spontaneous curvature. At a first glance this model, related to the theory of the smectic liquid crystals [43], completely disregards the elastic properties of the membrane interior, however, a closer inspection (see Appendix 10A) shows that the latter effect is implicitly accounted for by the surface free energy. The model by Dan et al. gives predictions about the membrane shape and the interaction between two protein inclusions; generally both the calculated shapes and interaction turn out to be non-monotonic (oscillatory) [38,40]. The comparison between theory and experiment can be realized through the radial correlation function of the protein distribution throughout the membrane, which is simultaneously liable to measurement and calculation, once the interaction potential is available [40]. Unfortunately, for the time being it is not possible to achieve an actually quantitative comparison between theory and experiment because (i) there are no appropriate experimental sets of data and (ii) the values of the model parameters are not certainly known.

The conclusions that the lipid hydrocarbon tails in a bilayer are subjected to substantial mechanical stresses [10,11,13,44] does not contradict the experimental fact that usually the total tension of a lipid bilayer, γ_b, is rather low ($\gamma_b \ll 1$ mN/m). The low value of γ_b is due to the fact that considerable negative (compressing) stresses, localized at the membrane–water interfaces, are almost completely counterbalanced by strong positive (stretching) stresses in the

hydrocarbon-chain region, which are even able to cause conformational changes in the imbedded proteins [44]. One could expect an impact of this internal non-uniform stress distribution (neglected in Refs. [38-40]) on the lipid mediated protein-protein interaction. This was a part of our motivation to propose in Ref. [45] an appropriate "sandwich" model of the lipid membrane, which is presented in the next Section 10.2, and further applied to describe the bilayer shape (Section 10.3) and the lateral force between two inclusions (Section 10.4).

10.2. "SANDWICH" MODEL OF A LIPID BILAYER

10.2.1. DEFINITION OF THE MODEL; STRESS BALANCES IN A LIPID BILAYER AT EQUILIBRIUM

A lipid bilayer drawn to scale is shown in Fig. 10.2. One can distinguish a hydrophobic hydrocarbon chain region sandwiched between two hydrophilic regions of the lipid polar headgroups. Recent studies [6, 46] indicate that the headgroup region can be more voluminous than it is depicted in Fig. 10.2. It is generally accepted that from a mechanical viewpoint a lipid bilayer behaves as a *two-dimensional viscous fluid* at body temperature. This two-dimensional fluidity is manifested when inclusions are moving throughout the membrane [47]. On the other hand, the bilayer exhibits *elastic* properties in processes of dilatation or bending, both of them being accompanied by extension or compression of the hydrocarbon chains of the lipids.

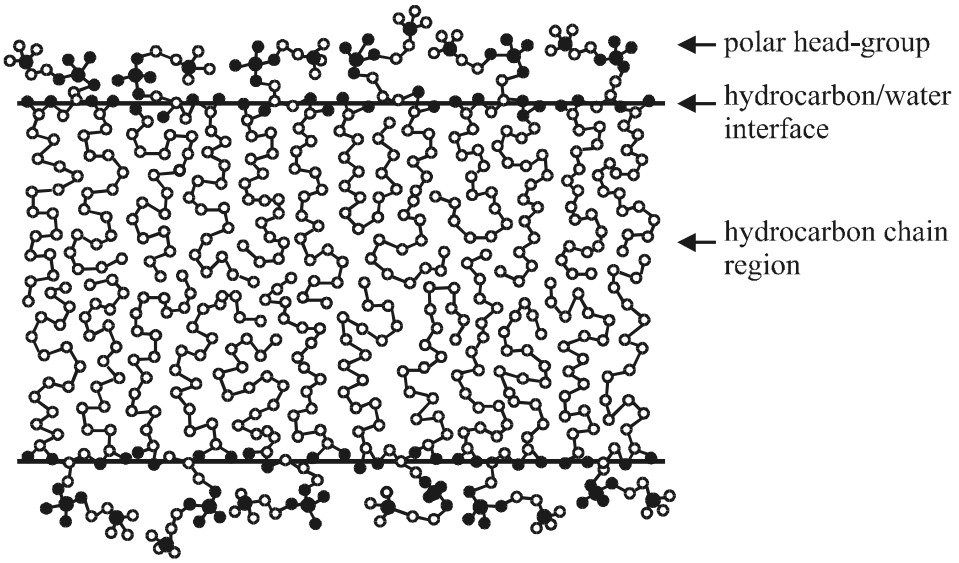

Fig. 10.2. A lipid (lecithin) bilayer drawn to scale; after Ref. [50].

In other words, a bilayer can exhibit different rheological behavior (fluid, elastic or hybrid) depending on the mode of deformation. This is not surprising, because a bilayer is neither a three-dimensional, nor a two-dimensional continuum and the hydrocarbon region is neither an isotropic liquid, nor a solid.

The generally accepted theoretical model treats a thin liquid film as a liquid layer confined between two Gibbs dividing surfaces, whose interaction is accounted for by an excess disjoining pressure (surface force per unit area) [48-50].

In Ref. [45] the thin-film approach has been extended to phospholipid bilayers (membranes). The hydrocarbon interior of the bilayer has been mechanically described as an elastic medium (rather than as a liquid), which is sandwiched between two Gibbs dividing surfaces modeling the two head-group regions, cf. Fig. 10.2. As already mentioned, in this chapter we present the description of the stresses in a lipid membrane provided by this *sandwich model*, as well as its application to quantify the interaction between two inclusions (like those depicted in Fig. 10.1).

Every deformation represents a change in the state of the bilayer with respect to some initial *reference state*. Following Ref. [45] we will consider the reference state to be a plane-parallel bilayer, formed as a result of self-assembly of lipid molecules. Due to the specific state of their hydrocarbon chains built into the bilayer, some internal stresses exist in the chain region [10,11,13,44]. They can be modeled by stresses in an elastic medium. In analogy with the micromechanical approach to the interfaces and thin films, see Eq. (1.4), one can express the pressure tensor in the chain region in the form

$$\mathbf{P} = P_T(\mathbf{e}_x\mathbf{e}_x + \mathbf{e}_y\mathbf{e}_y) + P_N\mathbf{e}_z\mathbf{e}_z \ , \tag{10.1}$$

see Fig. 10.3 for the notation. As in the case of thin liquid films the bilayer (film) surface tension σ can be defined as an excess with respect to the tangential component of the pressure tensor [51]:

$$\sigma = -\int_0^{h/2}[P_T^{\text{real}}(z) - P_T]dz - \int_{h/2}^{\infty}[P_T^{\text{real}}(z) - P_0]dz \tag{10.2}$$

where h is the thickness of the hydrocarbon chain region, P_T^{real} is the tangential component of

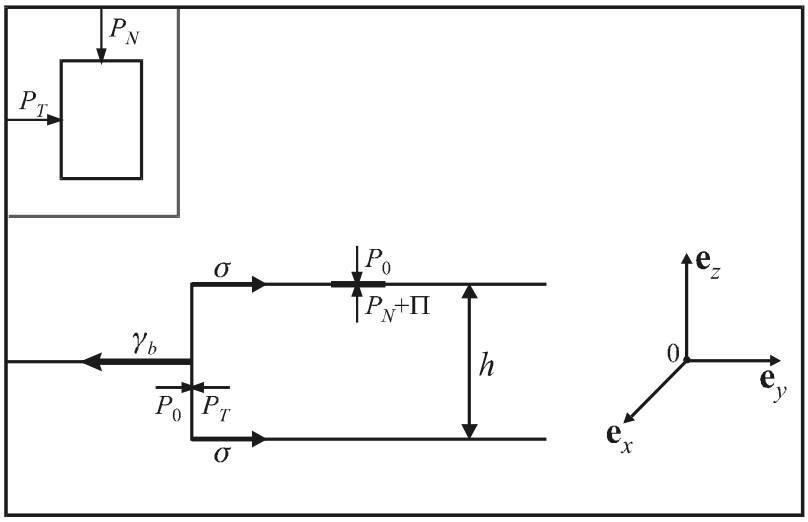

Fig. 10.3. Force balances in the reference state of a lipid bilayer modeled as an elastic medium; P_N and P_T are the normal and tangential components of the pressure tensor exerted on an element of the medium (the inset). Normal balance: the outer pressure P_0 is counterbalanced by the sum of P_N and the disjoining pressure Π. Tangential balance: the total bilayer tension γ_b is a superposition by the compressive surface tension σ at the membrane surfaces and the repulsive effect of the stresses in the bilayer interior, $(P_T - P_0)h$, where h is the thickness of the hydrophobic core; $\mathbf{e}_x$, $\mathbf{e}_y$, and $\mathbf{e}_z$ are the unit vectors of the coordinate axes.

the real pressure tensor and P_0 is the pressure in the bulk of the aqueous phase; P_N and P_T are attributes of the model, which can be determined as follows [45]. At equilibrium the force balance per unit area of the membrane surface is (see Fig. 10.3)

$$P_0 = P_N + \Pi \tag{10.3}$$

where, as usual, Π is the disjoining pressure accounting for the excess molecular interactions across the film [48-51]. Since the hydrocarbon chain region is a non-polar medium, one can expect that the value of Π will be determined mostly by the attractive van der Waals (dispersion) surface force, i.e.

$$\Pi = -\frac{A_{\mathrm{H}}}{6\pi h^3} \tag{10.4}$$

where A_{H} is the Hamaker constant see Chapter 5 and Refs. [49,50,52]. For a hydrocarbon film in water $A_{\mathrm{H}} \approx 10^{-20}$ J [50]; then with h = 3 nm one obtains $\Pi \approx -2 \times 10^4$ Pa. Using the value $P_0 \approx 10^5$ Pa (the atmospheric pressure), from Eq. (10.3) one estimates $P_N \approx 1.2 \times 10^5$ Pa [45].

In addition to the normal force balance, Eq. (10.3), we consider also the tangential force balance. As seen in Fig. 10.3, the stresses acting in lateral direction are related to σ and P_T. The total tension γ_b characterizes the bilayer as a membrane of zero thickness intervening between two aqueous phases of pressure P_0. Then in view of Fig. 10.3 one can write [45]

$$\gamma_b = 2\sigma + (P_0 - P_T)h \tag{10.5}$$

Equation (10.5) is in fact a form of the Rusanov equation, which has been originally derived for a thin liquid film [53]. The substitution of Eq. (10.2) into (10.5) yields

$$\gamma_b = -\int_{-\infty}^{+\infty}[P_T^{real}(z) - P_0]dz \tag{10.6}$$

Equation (10.6) shows that γ_b does not depend on the parameters of the model, such as the film thickness h. On the other hand, σ and P_T depend on the specific definition of the model. However, once this definition has been made, all parameters have well defined values for a given state of the real system. Such a situation is typical for the thermodynamics of thin liquid films [51].

One possibility to specify the model is to identify the bilayer surface tension σ with the interfacial tension of a lipid *adsorption monolayer* on a hydrocarbon-water interface at the same temperature, composition of the aqueous phase and area per lipid molecule as for the bilayer [45]. Indeed, the surface tension of the bilayer σ is expected to depend mostly on the interactions in the polar head-group region (Fig. 10.2) and to be insensitive to the state of the hydrocarbon interior. Actually, the experiments with dense lipid monolayers on hydrocarbon-water interface show that the interfacial tension does not depend on the length of the hydrocarbon chains of the lipids at varying area per molecule [54]. Therefore, identifying the surface tension of the *bilayer*, σ, with the interfacial tension of the respective *monolayer* at an oil–water interface, one subtracts the contribution from the interactions in the head-group region from the total membrane tension, γ_b, and consequently, attributes the excess stresses in the chain region to the tangential stress P_T:

$$(P_0 - P_T)h = \gamma_b - 2\sigma \tag{10.7}$$

see Eq. (10.5). In other words, having once σ defined, Eq. (10.7) determines the other parameter of the model, P_T. Often the lipid membranes are flaccid and their tension γ_b is rather low: $\gamma_b << 2\sigma$; this is usually quoted as the *tension free state* [15]. Equation (10.7) gives a simple interpretation of the tension free state ($\gamma_b \to 0$), viz. the lateral *compressing* force (per unit length) in the two head-group regions of the bilayer, 2σ (which is mostly due to the tendency to decrease the area of hydrocarbon-water contact), is counterbalanced by the lateral *repulsive* stress in the chain region, $(P_T - P_0)h$ [44,45].

As a numerical example let us take the experimental value $\sigma = 14$ mN/m from Ref. [54] for area 67 Å^2 per molecule of 1,2-distearoyl lecithin monolayer at the heptane-water interface. For a flaccid lipid bilayer

$$P_T \approx P_0 + 2\sigma / h \qquad (\gamma_b << 2\sigma) \qquad (10.8)$$

Then taking again $P_0 \approx 10^5$ Pa and $h = 3$ nm, one calculates $P_T \approx 9.4 \times 10^6$ Pa [45].

An inclusion (like these depicted in Fig. 10.1) generates deformations (strains) and creates additional stresses in the surrounding portion of the lipid membrane. As mentioned earlier, the overlap of the deformations caused by two inclusions is expected to give rise to a lateral force, which is analogous to the capillary immersion force described in Chapter 7. The difference with the common immersion force stems from the complicated rheology of the lipid membrane: neither liquid film nor elastic plate. A natural approach to the mechanics of such complex body is to use different constitutive relations (connecting stress and strain) for the different independent modes of deformation. The displacement vector **u** can be expressed as a sum of components due to the independent modes [45]:

$$\mathbf{u} = \mathbf{u}_{\text{stretching}} + \mathbf{u}_{\text{bending}} + \mathbf{u}_{\text{squeezing}} \qquad (10.9)$$

In the cases of uniform stretching and bending the bilayer behaves as an incompressible elastic body. However, in the case of a "squeezing" (peristaltic) deformation, which consists in a variation of bilayer thickness at immobile bilayer midplane (like it is in Fig. 10.1), the two-dimensional fluidity of the lipid membrane shows up, see Section 10.3 below. In the next two Sections, 10.2.2 and 10.2.3, following Ref. [45] we will consider briefly the modes of *uniform*

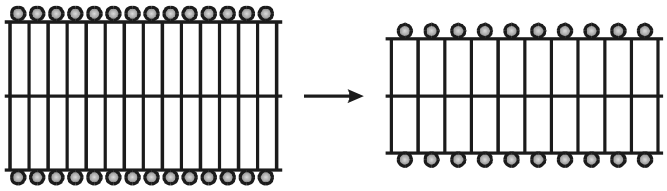

Fig. 10.4. The uniform stretching of a lipid bilayer results in a change of the shape of the hydrocarbon portion of each molecule (sketched as rectangle) at constant volume; after Ref. [45].

stretching and *bending*. Further, in Section 10.3, we pay special attention to the *squeezing mode*, which is related to the lateral interactions between membrane proteins.

10.2.2. STRETCHING MODE OF DEFORMATION AND STRETCHING ELASTIC MODULUS

Deformation of uniform stretching is presented schematically in Fig. 10.4. Each rectangle symbolizes the hydrocarbon portion of a lipid molecule, which is considered as an *incompressible elastic* body; the shadowed circles symbolize the headgroups. Lateral slip between the neighboring "rectangles" is allowed, which reflects the two-dimensional fluidity of the bilayer. The stretching results in a change of the shape of the hydrocarbon portion of each molecule at constant volume (Fig. 10.4). This deformation is not accompanied with a lateral slip between the neighboring lipid molecules. Therefore, in this case the two-dimensional fluidity does not show up and the hydrocarbon interior of the membrane can be treated as an elastic medium, see e.g. Ref. [55].

Let us denote by ΔP_N and ΔP_T the changes in P_N and P_T, which are due to the stretching of the bilayer. Following Chapter 5 of the book by Landau and Lifshitz [55] for a deformation of uniform stretching one can derive

$$\tau_{xx} = \tau_{yy} = -\Delta P_T\,; \qquad \tau_{zz} = -\Delta P_N\,, \tag{10.10}$$

where τ_{ij} $(i,j = x, y, z)$ are components of the *stress* tensor (the stress equals the negative pressure by definition). The components of the *strain* tensor are defined as follows [55]:

$$u_{ij} = \frac{1}{2}\left(\frac{\partial u_j}{\partial x_i} + \frac{\partial u_i}{\partial x_j}\right), \qquad (x_1 = x,\ x_2 = y,\ x_3 = z) \tag{10.11}$$

where u_i ($i = x, y, z$) is a component of the displacement vector **u**. For an elastic body the connections between strain and stress are given by Eq. (4.8) in Ref. [55], which in view of our Eq. (10.10) acquires the form [45]:

$$u_{zz} = -\frac{1}{9K_e}(\Delta P_N + \Delta P_T) - \frac{1}{3\lambda}(\Delta P_N - \Delta P_T) \tag{10.12}$$

$$u_{xx} = u_{yy} = -\frac{1}{9K_e}(\Delta P_N + \Delta P_T) + \frac{1}{6\lambda}(\Delta P_N - \Delta P_T) \tag{10.13}$$

Here K_e is the elastic compressibility modulus and λ is the coefficient of shear elasticity. For a liquid-like medium $K_e >> \lambda$, i.e. such a medium can be regarded as being incompressible. In addition, the terms $(\Delta P_N - \Delta P_T)$ and $(\Delta P_N + \Delta P_T)$ have the same order of magnitude (it turns out that $|\Delta P_T| >> |\Delta P_N|$, see Ref. [45] for more details). Hence the terms proportional to $1/K_e$ in Eqs. (10.12)–(10.13) can be neglected:

$$u_{xx} = u_{yy} = -\frac{1}{2}\ u_{zz} = \frac{1}{6\lambda}(\Delta P_N - \Delta P_T) \tag{10.14}$$

The components of the strain tensor determined by Eq. (10.14) obey the incompressibility condition $\nabla\cdot\mathbf{u} = 0$, which in view of Eq. (10.11) takes the form $u_{xx} + u_{yy} + u_{zz} = 0$. Further, let A and ΔA be the area of the bilayer and its change in the course of deformation. Then the relative dilatation (stretching) of the bilayer is [45]

$$\alpha \equiv \Delta A/A = u_{xx} + u_{yy} \tag{10.15}$$

Likewise, the relative change in the thickness is

$$\Delta h/h = u_{zz} = -\alpha\,, \tag{10.16}$$

where we have used the incompressibility condition. The stretching elastic modulus of the lipid bilayer (membrane) K_s is defined by the relationship [15]

$$\Delta\gamma_b = K_s\alpha \tag{10.17}$$

where $\Delta\gamma_b$ is the increment of the membrane tension γ_b due to the dilatation α. To obtain an expression for K_s in the framework of the "sandwich" model we differentiate Eq. (10.5):

$$\Delta\gamma_b = 2\Delta\sigma + (P_0 - P_T)\Delta h - h\Delta P_T \tag{10.18}$$

The differentiation of Eqs. (10.3) and (10.4) yields $\Delta P_N = -\Delta\Pi = 3\Pi\Delta h/h = -3\Pi\alpha$, see Eq. (10.16). Then from Eqs. (10.14) and (10.15) one obtains

$$\Delta P_T = \Delta P_N - 3\lambda\alpha = -3(\Pi + \lambda)\alpha \tag{10.19}$$

Further, in linear approximation one can write

$$\Delta\sigma = E_G\alpha \tag{10.20}$$

where E_G is the Gibbs elasticity of a lipid monolayer, cf. Eq. (1.45) and Table 1.2. Finally, in Eq. (10.18) we substitute $\Delta\sigma$ from Eq. (10.20), $(P_0 - P_T)$ from Eq. (10.8), Δh from Eq. (10.16) and ΔP_T from Eq. (10.19); as a result we obtain Eq. (10.17) in which K_s is determined by the following expression [45]:

$$K_s = 2\sigma + 2E_G + 3\Pi h + 3\lambda h \qquad \text{(stretching elastic modulus)} \tag{10.21}$$

The term $2\sigma + 2E_G$ in Eq. (10.21) accounts for the elastic response of the two membrane surfaces, whereas the term $3\Pi h + 3\lambda h$ represents a correction related to the internal hydrocarbon chain region. Using the numerical values given after Eq. (10.4) one estimates $3\Pi h \approx 0.18$ mN/m, which is much smaller than the total value of K_s, which can be of the order of 100 mN/m. Fernandez-Puente et al. [56] estimated that the elasticity of the chain region contributes about 20 mN/m to the total stretching modulus K_s. If one can identify this contribution with the last term in Eq. (10.21), that is $3\lambda h = 20$ mN/m, then with $h = 3.6$ nm one calculates $\lambda \approx 2 \times 10^6$ Pa [45].

It should be noted that Eq. (10.17) describes the direct dilatation of the membrane. However, the real flaccid lipid membranes are corrugated by thermally excited undulations (capillary waves), and most frequently the average (projected) area of the membrane can be experimentally measured, see e.g. Ref. [57]. The projected area is predicted to increase through superposition of two dilatory effects: (i) suppression of the thermal undulations and (ii) direct elastic stretch of the molecular surface area; the corresponding generalized form of Eq. (10.17) reads [58]:

$$\alpha = \frac{kT}{8\pi k_t}\ln(1 + A\Delta\gamma_b/4\pi k_t) + \Delta\gamma_b/K_s \tag{10.17a}$$

where A is the membrane area, α is the dilatation of the projected membrane area and k_t is the total bending elastic modulus of the membrane as a whole (see the next Section 10.2.3). The experiment [57] confirms that for smaller dilatation (say $\alpha < 0.02$) $\ln(\Delta\gamma_b)$ is a linear function

of α as predicted by Eq. (10.17a), whereas for larger deformations (say $0.02 < \alpha < 0.05$) $\Delta\gamma_b$ grows linearly with α in agreement with Eq. (10.17); for $\alpha > 0.05$ the lipid membrane usually breaks. Equation (10.17a) describes the transition from "logarithmic" to "linear" regime of dilatation.

10.2.3. BENDING MODE OF DEFORMATION AND CURVATURE ELASTIC MODULI

We consider flexural deformations of a lipid bilayer (membrane) under the condition for small deviations from planarity. In such a case the work of flexural deformation per unit area, Δw_b, can be expressed in terms of the Helfrich [59] phenomenological expression

$$\Delta w_b = 2k_t H^2 + \bar{k}_t K \tag{10.22}$$

Here k_t is the bending elastic modulus of the bilayer as a whole; $\bar{k}_t$ is torsion or Gaussian curvature elastic modulus, H and K are the mean and the Gaussian curvatures of the bilayer midsurface, see Section 3.1.2 for details.

Below, following Ref. [45], we derive an equation of the type of Eq. (10.22) using the "sandwich" model of the lipid membrane, and then comparing the coefficients multiplying H^2 and K we obtain expressions for the curvature elastic moduli k_t and $\bar{k}_t$. In the framework of this model Δw_b can be presented in the form

$$\Delta w_b = \Delta w_s + \Delta w_{in}\,, \tag{10.23}$$

where Δw_s and Δw_{in} are contributions due to the bilayer surfaces and bilayer interior (chain region), respectively. The latter two contributions are considered separately below.

The flexural deformation of the bilayer interior can be characterized by the equation of the shape of the bilayer midplane:

$$z = \zeta(x,y), \tag{10.24}$$

see Fig. 10.5. The initial state is assumed to be a planar bilayer, like those depicted in Fig. 10.4. The bending of the hydrocarbon chain region will transform the "rectangles" in Fig. 10.4 into the "trapezia" in Fig. 10.5. The bilayer subjected to such deformation cannot exhibit its two dimensional fluidity (viscous slip between chains of neighboring lipids). For that reason the

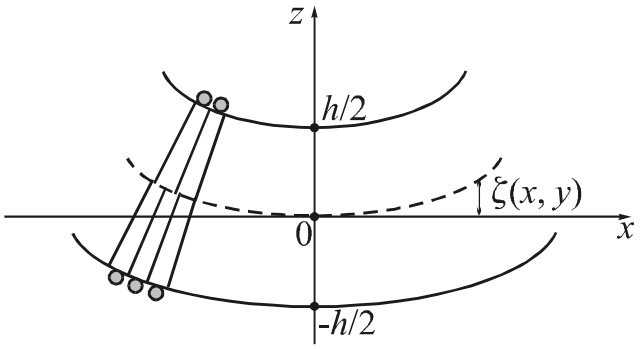

Fig. 10.5. Bending deformation of an initially planar lipid bilayer of thickness h; $z = \zeta(x,y)$ is the equation describing the shape of the bilayer midsurface after the deformation.

chain region can be treated as an incompressible *elastic* medium (elastic plate) when considering a purely flexural deformation [45]. Then one can use directly the expressions for the components of the strain tensor (in linear approximation) derived in Ref. [55], see Eq. (1.4) therein:

$$u_{xx} = -z\frac{\partial^2 \zeta}{\partial x^2}\ ; \qquad u_{yy} = -z\frac{\partial^2 \zeta}{\partial y^2}\ ; \qquad u_{xy} = -z\frac{\partial^2 \zeta}{\partial x \partial y}\ ; \tag{10.25}$$

$$u_{xz} = u_{yz} = 0, \qquad u_{zz} = z\left(\frac{\partial^2 \zeta}{\partial x^2} + \frac{\partial^2 \zeta}{\partial y^2}\right) \tag{10.26}$$

The relative dilatation of the lower and upper bilayer surfaces, α_1 and α_2, and the change in its thickness, Δh, are related to the components of the strain tensor by the expressions [45]:

$$\alpha_1 = (u_{xx} + u_{yy})\Big|_{z=-h/2}\ ; \qquad \alpha_2 = (u_{xx} + u_{yy})\Big|_{z=-h/2}\ ; \qquad \Delta h = \int_{-h/2}^{h/2} u_{zz}\, dz \tag{10.27}$$

Substituting u_{xx}, u_{yy} and u_{zz} from Eqs. (10.25)–(10.26) into Eq. (10.27) one obtains

$$\alpha_2 = -\alpha_1\ , \qquad \Delta h = 0\ , \tag{10.28}$$

which means that the lower surface is extended, the upper surface is compressed and the membrane thickness does not change (in linear approximation) during the considered flexural deformation. The stress tensor for an incompressible isotropic elastic medium is [55]

$$\tau_{ij} = 2\lambda\, u_{ij} \qquad (i, j = x, y, z) \tag{10.29}$$

where, as usual, λ is the coefficient of shear elasticity. The free energy per unit area of the bilayer is given by a standard expression from the theory of elasticity [55]:

$$\Delta w_{\text{in}} = \tfrac{1}{2} \int_{-h/2}^{h/2} \sum_{i,j} \tau_{ij} u_{ij}\, dz \tag{10.30}$$

Next we substitute Eqs. (10.25), (10.26) and (10.29) into Eq. (10.30) and after some transformations we obtain [60,55]:

$$\Delta w_{\text{in}} = \tfrac{2}{3} \lambda h^3 H^2 - \tfrac{1}{6} \lambda h^3 K\,, \tag{10.31}$$

where we have used the fact that in linear approximation the mean and Gaussian curvatures can be expressed as follows:

$$2H = \frac{\partial^2 \zeta}{\partial x^2} + \frac{\partial^2 \zeta}{\partial y^2}; \qquad K = \frac{\partial^2 \zeta}{\partial x^2} \frac{\partial^2 \zeta}{\partial y^2} - \left(\frac{\partial^2 \zeta}{\partial x \partial y} \right)^2 \tag{10.32}$$

Equation (10.31) gives the sought-for contribution of the bilayer *interior* to the work of flexural deformation.

The flexural deformation of the bilayer surfaces is accompanied by a change in the energy of the system, which can be derived from the thermodynamic expression for the work of interfacial deformation per unit area [cf. Eq. (3.1)]:

$$dw_{\text{s}} = \sum_{k=1,2} [\, \gamma_k\, d\alpha_k + \xi_k\, d\beta_k + B_k\, dH_k + \Theta_k\, dD_k] \tag{10.33}$$

Here $k = 1$ for the lower bilayer surface and $k = 2$ for the upper bilayer surface (Fig. 10.5); α_k and β_k are the relative dilatation and shear of the k-th surface; these deformations are related to the trace and deviator of the two-dimensional strain tensor ($u_{\mu\nu} \equiv d_{\mu\nu} \delta t$, see Section 4.2.2):

$$\alpha_k = a^{\mu\nu} u_{\mu\nu}\,, \qquad \beta_k = q^{\mu\nu} u_{\mu\nu}\,, \qquad \text{for } z = (-1)^k h/2 \qquad (\mu,\ \nu = x,\ y) \tag{10.34}$$

(k = 1, 2); $a^{\mu\nu}$ is the metric tensor in the respective curved surface, and $q^{\mu\nu}$ is its curvature deviatoric tensor [cf. Eq. (4.14)]:

$$q^{\mu\nu} = (b^{\mu\nu} - H_k\, a^{\mu\nu})/D_k \tag{10.35}$$

where $b^{\mu\nu}$ are components of the curvature tensor, $H_k = \tfrac{1}{2}(c_k^{(1)} + c_k^{(2)})$ and $D_k = \tfrac{1}{2}(c_k^{(1)} - c_k^{(2)})$ are the mean and deviatoric curvatures of the respective bilayer surfaces with $c_k^{(1)}$ and $c_k^{(2)}$ being the two principal curvatures; B_k and Θ_k in Eq. (10.33) are the respective surface bending and torsion moments; γ_k and ξ_k are the *thermodynamic* surface tension and shearing tension,

which are related to the respective *mechanical* surface and shearing tensions, σ_k and η_k , as follows [see Eq.(4.81)]:

$$\gamma_k = \sigma_k + \tfrac{1}{2} B_k H_k + \tfrac{1}{2} \Theta_k D_k , \qquad \xi_k = \eta_k + \tfrac{1}{2} B_k D_k + \tfrac{1}{2} \Theta_k H_k , \tag{10.36}$$

In linear approximation Eq. (10.34)–(10.36) considerably simplify. First we note that $\Delta h = 0$, cf. Eq. (10.28), and then [45]

$$-H_1 = H_2 = H , \qquad -D_1 = D_2 = D , \tag{10.37}$$

where H and D refer to the bilayer midsurface; the curvatures of the two bilayer surfaces have the opposite sign because the z-projections of the respective outer surface normals, directed from the chains toward the head-groups, have the opposite signs. In general, $D^2 = H^2 - K$, see Eq. (3.4); then using Eq. (10.32) in linear approximation one obtains

$$D^2 = \frac{1}{4}\left(\frac{\partial^2 \zeta}{\partial x^2} - \frac{\partial^2 \zeta}{\partial y^2} \right)^2 + \left(\frac{\partial^2 \zeta}{\partial x \partial y} \right)^2 \tag{10.38}$$

Further, in linear approximation the components of the curvature tensor are

$$b^{\mu\nu} = b_{\mu\nu} = \frac{\partial^2 \zeta}{\partial x_\mu \partial x_\nu} \qquad (x_1 = x;\ x_2 = y) \tag{10.39}$$

As known (Section 3.1.2), $2H$ and K, are equal to the trace and determinant of the curvature tensor $b^{\mu\nu}$, cf. Eqs. (10.32) and (10.39). Substituting Eqs. (10.25) and (10.35) into Eq. (10.34) and using Eqs. (10.32) and (10.37)–(10.39) one can derive [45]

$$\alpha_k = -hH_k ; \qquad \beta_k = -hD_k ; \qquad k = 1, 2. \tag{10.40}$$

Not only the bilayer as a whole, but also its surfaces can be considered as Helfrich surfaces, for which the energy of flexural deformation (per unit area) can be expressed in the form

$$w_f = 2k_c(H - H_0)^2 + \bar{k}_c K \tag{10.41}$$

Here k_c and $\bar{k}_c$ are the bending and torsion curvature elastic moduli for the film surfaces; H_0 is their "spontaneous curvature". Differentiating Eq. (10.41) and using the identity $K = H^2 - D^2$ one obtains

$$B_k = \left[\left(\frac{\partial w_f}{\partial H}\right)_D\right]_{H=H_k} = B_0 + 2(2k_c + \bar{k}_c)H_k\,, \qquad \Theta_k = \left[\left(\frac{\partial w_f}{\partial D}\right)_H\right]_{D=D_k} = -2\bar{k}_c D_k \qquad (10.42)$$

where $B_0 = -4k_cH_0$ is the bending moment of a planar bilayer surface, see Eq. (3.10). The expressions for B_k and Θ_k in Eq. (10.42) can be considered as truncated power expansions for low curvature. Of course, B_0 cannot depend on H_k, but it can depend on the surface dilatation α_k [45]:

$$B_0(\alpha) = B_{00} + \left(\frac{\partial B_0}{\partial \alpha}\right)_{\alpha=0} \alpha_k + O(\alpha_k^2) \qquad (10.43)$$

Next, combining Eqs. (10.40) and (10.43) with Eq. (10.42) we obtain the linear approximation for the bending moment B_k:

$$B_k = B_{00} + (4k_c + 2\bar{k}_c - B_0' h)H_k\,; \qquad B_0' \equiv \left(\frac{\partial B_0}{\partial \alpha}\right)_{\alpha=0} \qquad (10.44)$$

The mechanical surface tension σ_k also depends on both dilatation and curvature; in linear approximation one obtains $\sigma_k = \sigma_0 + E_G\alpha_k + \frac{1}{2}B_{00}H_k$, where the last term is often called the "Tolman term", see Eq. (4.87). Then in linear approximation Eq. (10.36) acquires the form

$$\gamma_k = \sigma_0 + E_G\alpha_k + B_{00}H_k\,, \qquad \xi_k = \tfrac{1}{2}B_{00}D_k\,, \qquad (10.45)$$

where we have used Eqs. (10.42) and (10.44) and have substituted $\eta = 0$ for a fluid interface (isotropic *two*-dimensional stress tensor). Further, using Eqs. (10.37), (10.40) and (10.45) we obtain the contributions from the dilatation and shearing into the work of surface deformation:

$$\sum_{k=1,2} \int_0^{\alpha_k} \gamma_k\, d\alpha_k = (E_G h^2 - B_{00}h)H^2; \qquad \sum_{k=1,2} \int_0^{\beta_k} \xi_k\, d\beta_k = -\tfrac{1}{2}B_{00}hD^2 \qquad (10.46)$$

Likewise, using Eqs. (10.37), (10.42) and (10.44) we obtain the contributions from the bending and torsion into the work of surface deformation:

$$\sum_{k=1,2} \int_0^{H_k} B_k\, dH_k = (4k_c + 2\bar{k}_c - B_0' h)H^2; \qquad \sum_{k=1,2} \int_0^{D_k} \Theta_k\, dD_k = -2\bar{k}_c D^2 \qquad (10.47)$$

Next, we integrate Eq. (10.33) and substitute Eqs. (10.46)–(10.47); using again the identity $D^2 = H^2 - K$ we present the result into the form [45]:

$$\Delta w_s = [4k_c - (\tfrac{3}{2}B_{00} + B_0')h + E_G h^2]H^2 + (2\bar{k}_c + \tfrac{1}{2}B_{00}h)K \tag{10.48}$$

Finally, we substitute Eqs. (10.31) and (10.48) into Eq. (10.23) and compare the result with Eq. (10.22); thus we obtain the sought-for expressions for the curvature elastic moduli of the bilayer as a whole [45]:

$$k_t = 2k_c - (\tfrac{3}{4}B_{00} + \tfrac{1}{2}B_0')h + \tfrac{1}{2}E_G h^2 + \tfrac{1}{3}\lambda h^3 \qquad \text{(bending elastic modulus)} \tag{10.49}$$

$$\bar{k}_t = 2\bar{k}_c + \tfrac{1}{2}B_{00}h - \tfrac{1}{6}\lambda h^3 \qquad \text{(torsion elastic modulus)} \tag{10.50}$$

The first terms in the right-hand sides of Eqs. (10.49) and (10.50), $2k_c$ and $2\bar{k}_c$, obviously stem from the bending and torsion elasticities of the two bilayer surfaces; the terms with $B_{00}h$ and $B_0' h$ are contributions from the bending moment (spontaneous curvature) of the these surfaces; the contribution of the surface (monolayer) elasticity $\frac{1}{2}E_G h^2$ in Eq. (10.49) was first obtained by Evans and Skalak [15], who derived $k_t = \frac{1}{2}E_G h^2$ by means of model considerations; the term proportional to λh^3 accounts for the elastic effect of the bilayer interior (the hydrocarbon-chain region).

In Ref. [45] typical parameter values have been used to estimate the magnitude of the contributions of the various terms in Eqs. (10.49) and (10.50): h = 3.6 nm, E_G = 40 mN/m, $\lambda = 3 \times 10^6$ Pa, $B_{00} = 7 \times 10^{-11}$ N, $k_c = 4 \times 10^{-21}$ J; to estimate $\bar{k}_c$ the relationship $\bar{k}_c = -\frac{1}{2}k_c$ from Refs. [61,62] can be used; then $\bar{k}_c \approx -5 \times 10^{-22}$ J; finally, B_0' can be assessed by means of the connection between B_0 and the ΔV (Volta) potential [62] assuming that the value of B_0' is determined mostly by electrostatic interactions [45]:

$$B_0' \equiv \frac{\partial B_0}{\partial \alpha} \approx \frac{\varepsilon}{4\pi}\Delta V \frac{\partial \Delta V}{\partial \alpha} \approx -3.2 \times 10^{-11}\,\text{N} \tag{10.51}$$

At the last step experimental data for the dependence of ΔV vs. α for dense lipid monolayers have been used: from Fig. 3 in Ref. [63] one obtains $\Delta V \approx 350$ mV, $\partial \Delta V/\partial \alpha \approx -323$ mV; dielectric constant $\varepsilon \approx 32$ has been adopted for the headgroup region. [When using Eq. (10.51) ΔV must be substituted in CGSE units, i.e. the value of ΔV in volts must be divided by 300.]

With the above parameters values one can estimate the magnitude of the various terms in Eqs. (10.49) and (10.50); below we list their values ($\times 10^{-19}$ J):

$$k_t \approx 1.83; \quad 2k_c \approx 0.08; \quad -(\tfrac{3}{4}B_{00} + \tfrac{1}{2}B_0')h \approx -1.31; \quad \tfrac{1}{2}E_G h^2 \approx 2.59; \quad \tfrac{1}{3}\lambda h^3 \approx 0.47 \qquad (10.52)$$

$$\bar{k}_t \approx 0.99; \quad 2\bar{k}_c \approx -0.04; \quad \tfrac{1}{2}B_{00}h \approx 1.26; \quad -\tfrac{1}{6}\lambda h^3 \approx -0.23 \qquad (10.53)$$

One sees that the value of k_t is determined mostly by the competition between the positive surface stretching elasticity term, $\frac{1}{2}E_G h^2$, and the negative surface bending moment term $-(\frac{3}{4}B_{00} + \frac{1}{2}B_0')h$. On the other hand, the value of $\bar{k}_t$ is dominated by the positive surface bending moment term, $\frac{1}{2}B_{00}h$. The chain elasticity contribution $\propto \lambda h^3$ is about 25% of the magnitude of k_t and $\bar{k}_t$, which is consonant with the discussion in Ref. [56].

In summary, the "sandwich" model provides expressions for calculating the stretching, bending and torsion elastic constants, K_s, k_t and $\bar{k}_t$, in terms of the chain elasticity constant λ and of the properties of the respective lipid *monolayers* at oil-water interface (E_G, B_{00}, B_0', k_c, $\bar{k}_c$, etc.), see Eqs. (10.21), (10.49) and (10.50). The estimates show that the quantitative predictions of the model are reasonable, although additional experiments are necessary to determine more precisely the values of the parameters.

10.3. DESCRIPTION OF MEMBRANE DEFORMATIONS CAUSED BY INCLUSIONS

10.3.1. SQUEEZING (PERISTALTIC) MODE OF DEFORMATION: RHEOLOGICAL MODEL

The deformation of a lipid bilayer around a cylindrical inclusion (say a transmembrane protein), having a hydrophobic belt of width l_0, represents a variation of the bilayer thickness at planar midplane (Fig. 10.6). Such a mode of deformation corresponds to the *squeezing* (peristaltic) mode observed with thin liquid films [64]. This type of deformation appears if there is a "mismatch", $h_c \equiv (l_0 - h)/2 \neq 0$, between the hydrophobic zones of the inclusion and bilayer; here, as usual, h is the thickness of the non-disturbed bilayer far from the inclusion. The extension of the lipid hydrocarbon chains along the z-axis is greater for molecules situated closer to the inclusion (Fig. 10.6). The chain region of a separate lipid molecule (one of the

many small rectangles depicted in Fig. 10.6) exhibits an elastic response to extension-compression; therefore it can be modeled as a stretchable elastic body of fixed volume. On the other hand, lateral slip between molecules (neighboring rectangles in Fig. 10.6) is not accompanied with any elastic effects because of the two-dimensional fluidity of the membrane. Both these properties are accounted for in the following mechanical constitutive relation for the stress tensor τ_{ij} [45]:

$$\tau_{zz} = 2\lambda \frac{\partial u_z}{\partial z}; \qquad \tau_{ij} = -p\delta_{ij}, \qquad (i,j) \neq (z,z) \qquad i,j = x,y,z \tag{10.54}$$

Here δ_{ij} is the Kroneker symbol, p has the meaning of pressure characterizing the bilayer as a two-dimensional fluid; u_z is the z-component of the displacement vector **u**; the coordinate system is depicted in Fig. 10.6. The above relationship between τ_{zz} and $\partial u_z/\partial z$ is a typical constitutive relation for an elastic body, cf. Eqs. (10.11) and (10.29). On the other hand, the tangential stresses τ_{ij} ($i, j = x, y$) in Eq. (10.54) are isotropic as it should be for a two-dimensional fluid. The condition for hydrostatic equilibrium and the continuity equation yield [55]:

$$\frac{\partial \tau_{ij}}{\partial x_i} = 0, \qquad j = 1,2,3; \qquad \nabla \cdot \mathbf{u} = 0 \qquad (x_1 = x,\ x_2 = y,\ x_3 = z), \tag{10.55}$$

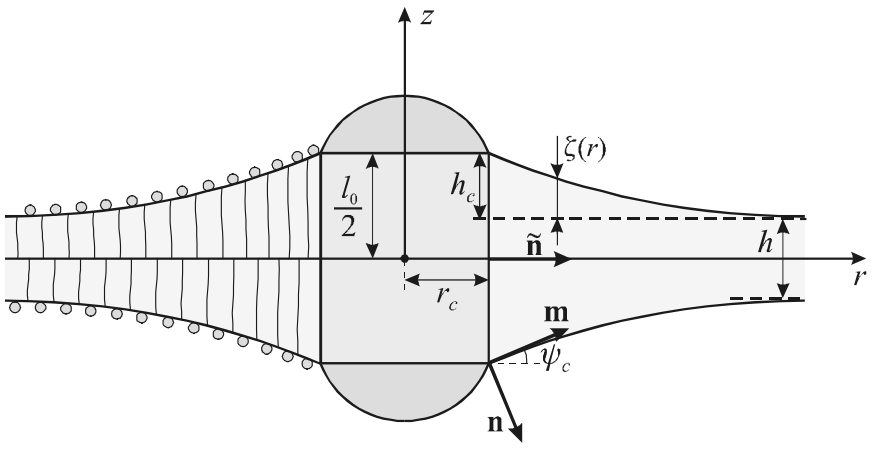

Fig. 10.6. Sketch of the deformation around a cylindrical inclusion (membrane protein) of radius r_c and width of the hydrophobic belt l_0; h is the thickness of the non-disturbed bilayer; ζ is the perturbation in the bilayer thickness caused by the inclusion; h_c is the mismatch between the hydrophobic regions of the inclusion and the bilayer; **n** and **ñ** are unit vectors normal to the membrane surface and inclusion surface, respectively; **m** is unit vector in direction of the bilayer surface tension.

where τ_{ij} is to be substituted from Eq. (10.54); as usual, summation over the repeated indices is assumed. In this way, the mechanical problem is formulated: Eqs. (10.55) represent a set of 4 equations for determining the 4 unknown functions u_x, u_y, u_z and p. Below, following Ref. [45] we present the solution of this mechanical problem.

10.3.2. DEFORMATIONS IN THE HYDROCARBON-CHAIN REGION

Considerations of symmetry imply that u_z must be an odd function of z which has to satisfy the boundary condition

$$u_z = \zeta(x,y) \quad \text{for} \quad z = h/2, \tag{10.56}$$

where $z = \zeta(x,y)$ describes the shape of the upper bilayer surface, see Fig. 10.6. Equation (10.55) for $j = z$, along with Eq. (10.54), yields

$$\frac{\partial^2 u_z}{\partial z^2} = 0 \tag{10.57}$$

Combining Eqs. (10.56) and (10.57) one obtains

$$u_z = \frac{2z}{h}\ \zeta(x,y) \tag{10.58}$$

The continuity (incompressibility) equation $\nabla\cdot\mathbf{u} = 0$ can be expressed in the form

$$\nabla_{\text{II}}\cdot\mathbf{u}_{\text{II}} = -\frac{\partial u_z}{\partial z} \tag{10.59}$$

where $\mathbf{u}_{\text{II}}$ is the projection of the displacement vector $\mathbf{u}$ in the plane xy and, as usual, ∇_{II} is the gradient operator in the same plane:

$$\mathbf{u}_{\text{II}} = \mathbf{e}_x u_x + \mathbf{e}_y u_y\ ; \qquad \nabla_{\text{II}} = \mathbf{e}_x \frac{\partial}{\partial x} + \mathbf{e}_y \frac{\partial}{\partial y} \tag{10.60}$$

One can seek $\mathbf{u}_{\text{II}}$ in the form [45]

$$\mathbf{u}_{\text{II}} = -\nabla_{\text{II}}\, g(x,y,z) \tag{10.61}$$

where g is an unknown scalar function. The substitution of Eqs. (10.58) and (10.61) into Eq. (10.59) yields an equation for determining g :

$$\nabla_{\text{II}}^2 g = \frac{2}{h}\zeta \tag{10.62}$$

In addition, substituting Eq. (10.54) into (10.55) for $i, j = x, y$ gives $\nabla_{II} p = 0$, and consequently p is independent of x and y. Further, since τ_{ij} expresses a perturbation and the bilayer far from the inclusion(s) is not perturbed, one can conclude that p is identically zero [45]:

$$p \equiv 0 \tag{10.63}$$

To determine g from Eq. (10.62) one can use the boundary condition of impermeable inclusion surface [45]:

$$\tilde{\mathbf{n}}\cdot\mathbf{u}_{II} \equiv -\frac{\partial g}{\partial \tilde{n}} = 0 \qquad \text{(at the inclusion surface)} \tag{10.64}$$

Here $\tilde{\mathbf{n}}$ is an outer unit normal to the inclusion surface (Fig. 10.6) and $\partial g/\partial \tilde{n}$ is a directional derivative. Additional boundary conditions, which have to be imposed at the surfaces of the lipid bilayer, are considered below.

10.3.3. DEFORMATION OF THE BILAYER SURFACES

Since the bilayer surfaces are symmetric with respect to a planar midsurface (Fig. 10.6), it is sufficient to determine the shape $z = \zeta(x,y)$ of the upper bilayer surface. We do not impose any restrictions on the number and mutual positions of the cylindrical inclusions. The mechanical description can be based on the theory of liquid films of uneven thickness developed in Refs. [51,65]. In particular, we will employ the equation for the balance of all forces applied to the upper surface of such a film (the interfacial balance of the linear momentum) [51,65]:

$$\nabla_s\cdot\underline{\boldsymbol{\sigma}} - \mathbf{n}\cdot(\mathbf{T}_I - \mathbf{T}_{II})|_{z=h/2} + \Pi(\mathbf{e}_z\cdot\mathbf{n})\mathbf{e}_z = 0 \tag{10.65}$$

where $\underline{\boldsymbol{\sigma}}$ is the surface stress tensor (the usual surface tension is equal to a half of the trace of $\underline{\boldsymbol{\sigma}}$), ∇_s is the two-dimensional gradient operator of the film surface, which is to be distinguished from the gradient operator ∇_{II} in the plane xy (the midsurface); $\mathbf{n}$ is the running outer unit normal of the bilayer surface, which can be expressed in the form [65]

$$\mathbf{n} = (\mathbf{e}_z - \nabla_{II}\zeta)(1 + |\nabla_{II}\zeta|^2)^{-1/2} ; \tag{10.66}$$

$\mathbf{T}_I$ and $\mathbf{T}_{II}$ are respectively the stress tensors inside and outside the bilayer, which can be expressed in the form [45]:

$$\mathbf{T}_I = -P_N\,\mathbf{e}_z\,\mathbf{e}_z - P_T\,\mathbf{U}_{II} + \underline{\boldsymbol{\tau}} ; \qquad \mathbf{T}_{II} = -P_0\mathbf{U} ; \tag{10.67}$$

$\mathbf{U}$ is the spatial unit tensor, $\mathbf{U}_{II} \equiv \mathbf{e}_x \mathbf{e}_x + \mathbf{e}_y \mathbf{e}_y$ is the unit tensor in the plane xy, P_0 is the pressure in the aqueous phase, P_N and P_T characterize the stresses in a plane-parallel bilayer (see Fig. 10.3), the components τ_{ij} of the tensor $\underline{\boldsymbol{\tau}}$ are defined by Eq. (10.54); $\underline{\boldsymbol{\tau}}$ accounts for the additional stresses due to the deformation in the bilayer. The disjoining pressure Π is due to the conventional surface forces (like the van der Waals ones), whereas $\underline{\boldsymbol{\tau}}$ accounts for the elastic stresses. The general form of the surface stress tensor is [66,67]

$$\underline{\boldsymbol{\sigma}} = \mathbf{a}_\mu \mathbf{a}_\nu \sigma^{\mu\nu} + \mathbf{a}_\mu \mathbf{n} \sigma^{\mu(\mathrm{n})} \tag{10.68}$$

see Eq. (4.26); here and hereafter the Greek indices take values 1 and 2, summation over repeated indices is assumed, $\mathbf{a}_1$ and $\mathbf{a}_2$ are vectors of the surface local basis, which at each point are tangential to the bilayer surface; see Refs. [68,69] about the formalism of differential geometry; $\sigma^{\mu\nu}$ and $\sigma^{\mu(\mathrm{n})}$ are the respective components of the surface stress tensor; $\sigma^{\mu(\mathrm{n})}$ are known as surface transversal shear stress resultants [15]. Next, using Eqs. (10.66)–(10.68) one can obtain the normal and tangential projections of the vectorial balance, Eq. (10.65), with respect to the bilayer surface $z = \zeta(x,y)$ [45]:

$$b_{\mu\nu}\sigma^{\mu\nu} + \sigma^{\nu(\mathrm{n})}{}_{,\nu} = [(P_N - P_T)|\nabla_{II}\zeta|^2 - \Pi](1 + |\nabla_{II}\zeta|^2)^{-1} + \Pi_0 + \mathbf{n}\cdot\underline{\boldsymbol{\tau}}\cdot\mathbf{n} \tag{10.69}$$

$$\sigma^{\mu\nu}{}_{,\mu} - b^{\nu}{}_{\mu}\sigma^{\mu(\mathrm{n})} = (P_T - P_N - \Pi)(1 + |\nabla_{II}\zeta|^2)^{-1/2}\,\zeta^{,\nu} + \mathbf{n}\cdot\underline{\boldsymbol{\tau}}\cdot\mathbf{a}^{\nu} \qquad (\nu = 1, 2) \tag{10.70}$$

As before, $b_{\mu\nu}$ are components of the curvature tensor, the comma denotes covariant differentiation [68,69], and $\Pi_0 = P_0 - P_N$ is the disjoining pressure of the non-deformed plane-parallel bilayer. The normal projection of the stress balance, Eq. (10.69), presents a generalization of the Laplace equation of capillarity; it will be used below to determine the shape of the bilayer surface. The tangential projection, Eq. (10.70), allows one to determine the variation of the surface tension along the deformed surface; it will be utilized below to calculate the interaction between two inclusions.

First of all, we transform and simplify the normal projection of the surface force balance, Eq. (10.69). Because of the *two*-dimensional fluidity of the lipid bilayer, the surface stress tensor $\underline{\boldsymbol{\sigma}}$ must be tangentially isotropic [45]:

$$\sigma^{\mu\nu} = \sigma a^{\mu\nu} \qquad (a^{\mu\nu} = \mathbf{a}^{\mu}\cdot\mathbf{a}^{\nu}) \tag{10.71}$$

where σ is the usual scalar surface tension and $a^{\mu\nu}$ are components of the surface metric tensor [68,69]. Then one obtains

$$b_{\mu\nu}\sigma^{\mu\nu} = a^{\mu\nu}b_{\mu\nu}\sigma = 2H\sigma \approx \sigma\nabla_{\mathrm{II}}^2\zeta \tag{10.72}$$

At the last step we have used the fact that in linear approximation (for small ζ) the mean curvature is determined by the expression $2H \approx \nabla_{\mathrm{II}}^2\zeta$, cf. Eq. (10.32). In addition, just as in Chapters 7 and 9 for small deformations we will expand the disjoining pressure in series keeping the linear terms:

$$\Pi = \Pi_0 + 2\Pi'\zeta + \ldots ; \qquad \Pi' \equiv (d\Pi/dh)|_{\zeta=0} \tag{10.73}$$

To express the transverse shear stress resultants will employ an equation, which stems from the surface balance of the *angular* momentum, see Eq. (4.49) and Refs. [15,66,67,70]:

$$\sigma^{\mu(\mathrm{n})} = -M^{\mu\nu}{}_{,\nu} \tag{10.74}$$

Here $M^{\mu\nu}$ are components of the tensor of the surface moments (see Section 4.2.3), which can be expressed as a sum of isotropic and deviatoric parts [70,71]:

$$M^{\mu\nu} = \tfrac{1}{2}(B\,a^{\mu\nu} + \Theta\,q^{\mu\nu}) , \tag{10.75}$$

see also Eq. (10.35). For a Helfrich interface the bending and torsion moments, B and Θ, are given by Eq. (10.42); then Eq. (10.75) acquires the form

$$M^{\mu\nu} = [(2k_c + \bar{k}_c)H + B_0/2]a^{\mu\nu} - \bar{k}_c\,Dq^{\mu\nu} , \tag{10.76}$$

In view of Eq. (10.43) one obtains

$$B_0 \approx B_{00} + B_0'\,\alpha = B_{00} - (2B_0'/h)\zeta , \qquad \alpha = -2\zeta/h ; \tag{10.77}$$

the last expression for the dilatation α of the bilayer surface follows from Eqs. (10.11), (10.16) and (10.58). Next, we differentiate Eq. (10.76) with the help of Eqs. (10.35), (10.77) and the identity $b^{\mu\nu}{}_{,\nu} = 2H^{,\mu}$ [70]; as a result we obtain [45]

$$\sigma^{\mu(\mathrm{n})} = -M^{\mu\nu}{}_{,\nu} = -2k_c H^{,\mu} + (B_0'/h)\zeta^{,\mu} \tag{10.78}$$

Further, we substitute Eqs. (10.54), (10.58), (10.72), (10.73) and (10.78) into the normal stress balance, Eq.(10.69), to obtain its linearized form [45]

$$\widetilde{\sigma}_0 \nabla_{\text{II}}^2 \zeta - k_c \nabla_{\text{II}}^4 \zeta = 2(2\lambda/h - \Pi')\zeta; \qquad (\widetilde{\sigma}_0 \equiv \sigma_0 + B_0'/h) \tag{10.79}$$

where σ_0 is the value of σ for the non-disturbed plane-parallel bilayer. Equation (10.79) plays the role of a generalized Laplace equation for the bilayer surfaces.

10.3.4. The generalized Laplace equation for the bilayer surfaces

Equation (10.79) is a fourth order differential equation, which can be represented in the form [45]:

$$(\nabla_{\text{II}}^2 - q_2^2)(\nabla_{\text{II}}^2 - q_1^2)\zeta = 0 \tag{10.80}$$

Here q_1^2 and q_2^2 are roots of the biquadratic equation

$$k_c q^4 - \widetilde{\sigma}_0 q^2 + 2(2\lambda/h - \Pi') = 0 \tag{10.81}$$

which gives

$$q_{1,2}^2 = \{\widetilde{\sigma}_0 \pm [\widetilde{\sigma}_0^2 - 8k_c(2\lambda/h - \Pi')]^{1/2}\}/(2k_c) \tag{10.82}$$

Depending of the sign of the discriminant in Eq. (10.82), Eq. (10.81) may have four real or four complex roots for q. Complex q leads to decaying oscillatory profiles for $\zeta(x,y)$, resembling those obtained in Ref [38] for model inclusions of translational symmetry. For not-too-flaccid membranes the discriminant in Eq. (10.82) is positive,

$$\widetilde{\sigma}_0^2 > 8k_c(2\lambda/h - \Pi') \qquad \text{(real roots)} \tag{10.83}$$

In such case two positive roots for q^2 are obtained and the bilayer profile around an inclusion, $\zeta(x,y)$ in Fig. 10.6, will decay without oscillations. Using Eq. (10.4) one can estimate that Π' is typically about 2×10^{13} N/m^3 which is negligible compared with $2\lambda/h$. Indeed, with h = 3 nm and $\lambda = 2 \times 10^6$ N/m^2 one obtains $2\lambda/h = 1.33 \times 10^{15}$ N/m^3. Further, assuming $k_c \approx 4 \times 10^{-21}$ J (see Ref. [72]) from Eq. (10.83) one obtains $\widetilde{\sigma}_0 > 6.5$ mN/m. The latter inequality can be fulfilled for not-too-flaccid bilayers. Note that the bilayer surface tension σ_0, as introduced in Section 10.2.1 above, is usually much larger than the total tension of the bilayer, γ_b, see the discussion after Eq. (10.7); the importance of the surface tension σ_0 is discussed also at the end of Appendix 10A.

Following Ref. [45], below we will restrict our considerations to the case of *real* q^2, in which Eq. (10.83) is satisfied; the case of complex q^2 is also possible and physically meaningful. As in Chapter 7, here q^{-1} has the meaning of a characteristic capillary length determining the range of the deformation around an inclusion, and in turn, the range of the lateral capillary forces between inclusions (see below). With the above values of h, λ and k_c, and with $\widetilde{\sigma}_0$ = 20 mN/m from Eq. (10.82) two possible decay lengths can be calculated [45]: $q_1^{-1} = 2.7$ nm and $q_2^{-1} = 0.45$ nm. The second decay length, q_2^{-1}, is smaller than the size of the headgroup of a phospholipid molecule (typically 0.8 nm); for that reason this decay length has been disregarded in Ref. [45]. Below we will work with the other decay length, that is with

$$q^2 = q_1^2 = \{\widetilde{\sigma}_0 - [\widetilde{\sigma}_0^2 - 8k_c(2\lambda/h - \Pi')]^{1/2}\}/(2k_c) \approx 4\lambda/(h\widetilde{\sigma}_0) \tag{10.84}$$

At the last step we expanded the square root in series for small k_c. Disregarding the solution of Eq. (10.80) for $q = q_2$ means that we have to seek ζ as a solution of the equation [45]

$$\nabla_{\mathrm{II}}^2 \zeta = q^2 \zeta \tag{10.85}$$

where q is determined by Eq. (10.84). All solutions of Eq. (10.85) satisfy also Eq. (10.80). The boundary conditions for Eq. (10.85) are $\zeta = h_c$ at the lipid-protein boundary and $\zeta \to 0$ for $r \to \infty$, see Fig. 10.6. Note that Eq. (10.85) is almost identical to Eq. (7.6) with the only difference in the definitions of q. The account for the compressing stresses at the bilayer surfaces and the elastic stresses in the bilayer interior (see Section 10.2.1) leads to the appearance of the bilayer surface tension σ_0 and the chain shear elasticity λ in the expression for the decay length: $q^{-1} \approx (h\widetilde{\sigma}_0/4\lambda)^{1/2}$.

Comparing Eqs. (10.62) and (10.85) one can determine g [45]:

$$g = 2\zeta/(hq^2) + f(x, y, z), \tag{10.86}$$

$$\nabla_{\mathrm{II}}^2 f = 0 \tag{10.87}$$

Here f is unknown function (to be determined from the boundary conditions) which satisfies Eq. (10.87). Below we will determine ζ and f for the cases of one and two inclusions incorporated in a lipid membrane.

10.3.5. SOLUTION OF THE EQUATIONS DESCRIBING THE DEFORMATION

Single cylindrical inclusion. In this case ζ depends on the radial coordinate r (Fig. 10.6) and Eq. (10.85) acquires the form of a modified Bessel equation:

$$\frac{1}{r}\frac{d}{dr}\left(r\frac{d\zeta}{dr}\right) = q^2\zeta \tag{10.88}$$

The boundary condition for fixed position of the contact line implies

$$\zeta = h_c = \text{const.} \qquad \text{(at the contact line)} \tag{10.89}$$

The solution of Eq. (10.88), which satisfies Eq. (10.89) and decays at infinity is [45]:

$$\zeta = \frac{h_c}{\mathrm{K}_0(qr_c)}\mathrm{K}_0(qr), \qquad r \geq r_c \tag{10.90}$$

where r_c is the radius of the cylindrical inclusion (Fig. 10.6) and K_0 is the modified Bessel (Macdonald) function of zeroth order [73-75].

To completely quantify the deformation we have to determine also the components u_r and u_z of the displacement vector **u**. A substitution of Eq. (10.90) into Eq. (10.58) directly gives u_z. To find u_r we first substitute Eq. (10.86) into the boundary condition (10.64):

$$\left(\frac{2}{hq^2}\frac{d\zeta}{dr} + \frac{\partial f}{\partial r}\right)_{r=r_c} = 0 \tag{10.91}$$

Then from Eq. (10.87) we obtain [45]

$$f = A\ \ln r \tag{10.92}$$

The integration constant A can be determined from the boundary condition

$$\left(\frac{d\zeta}{dr}\right)_{r=r_c} = -\tan\psi_c = -qh_c\frac{\mathrm{K}_1(qr_c)}{\mathrm{K}_0(qr_c)} \tag{10.93}$$

where ψ_c is the surface slope at the contact line (Fig. 10.6). Next we substitute Eqs. (10.92) and (10.93) into Eq. (10.91) and determine

$$A = (2r_c\tan\psi_c)/(hq^2) \tag{10.94}$$

A substitution of ζ from Eq. (10.90) and f from Eq. (10.92) into Eq. (10.86) gives the function g, which is further substituted in (10.61) to obtain [45]

$$u_r = \frac{2h_c}{qh\mathrm{K}_0(qr_c)}\left[\mathrm{K}_1(qr) - \frac{r_c}{r}\mathrm{K}_1(qr_c)\right], \qquad u_\phi \equiv 0 \tag{10.95}$$

Finally, the components of the strain tensor (in cylindrical coordinates) can be obtained using standard formulas from Ref. [55]:

$$u_{rr} = \frac{\partial u_r}{\partial r}\ ; \quad u_{\phi\phi} = \frac{u_r}{r}\ ; \quad u_{zz} = \frac{\partial u_z}{\partial z} = \frac{2\zeta}{h}\ ; \quad u_{rz} = \frac{z}{h}\frac{\partial \zeta}{\partial r}\ ; \quad u_{r\phi} = u_{\phi z} = 0. \tag{10.96}$$

Couple of identical cylindrical inclusions. In this case it is convenient to introduce bipolar (bicylindrical) coordinates as explained in Section 7.2.1, see Eq. (7.25). Then Eq. (10.85) acquires the form

$$(\cosh\tau - \cos\omega)^2\left(\frac{\partial^2\zeta}{\partial\tau^2} + \frac{\partial^2\zeta}{\partial\omega^2}\right) = (qa)^2\zeta(\tau,\omega)\ ; \qquad a = (L^2/4 - r_c^2)^{1/2} \tag{10.97}$$

where L is the distance between the axes of the two cylindrical inclusions, see Fig. 10.1. In contrast with Section 7.2.1, here in general $(qa)^2$ is not a small parameter, and therefore we cannot use asymptotic expansions to find analytical solution of Eq. (10.97). The latter can be solved by numerical integration. The domain of integration is a rectangle in the $\omega\tau$-plane bounded by the lines $\omega = \pm\pi$ and $\tau = \pm\tau_c$, where $\tau_c = \ln[(a + L/2)/r_c]$, cf. Eq. (7.57). Owing to the symmetry one can carry out the numerical integration only in a quarter of the integration domain: $0 \le \tau \le \tau_c$ and $0 \le \omega \le \pi$. The boundary conditions are:

$$\zeta\Big|_{\tau=\tau_c} = h_c\ ; \qquad (\partial\zeta/\partial\tau)_{\tau=0} = (\partial\zeta/\partial\omega)_{\omega=0} = (\partial\zeta/\partial\omega)_{\omega=\pi} = 0 \tag{10.98}$$

In Ref. [45] the conventional second-order finite-difference scheme [75,76] has been used for discretization of the boundary problem. In this way Eq. (10.97) is presented as a system of linear equations, which can be solved by means of one of the standard methods. In Ref. [45] the Gauss-Seidel iterative method has been combined with successive over-relaxation (SOR) and Chebyshev acceleration technique, see e.g. Refs. [75-77].

Having calculated ζ, one obtains u_z from Eq. (10.58). In view of Eqs. (10.61) and (10.86) to determine the lateral projection of the displacement vector $\mathbf{u}_{\mathrm{II}}(\omega,\tau)$ from the calculated profile $\zeta(\omega,\tau)$ one is to first find the auxiliary function $f(\omega,\tau)$. The symmetry implies that $f(\omega,\tau)$ is an even function of both ω and τ. Moreover, since f obeys Eq. (10.87), it can be expressed as a Fourier cosine expansion [45]:

$$f(\omega,\tau) = \sum_{n=1}^{\infty} E_n \ \cosh n\tau \ \cos n\omega \tag{10.99}$$

The coefficients E_n are determined by substituting Eqs. (10.86) and (10,99) into the boundary condition $(\partial g/\partial\tau)_{\tau=\tau_c} = 0$, which follows from Eq. (10.64); thus one derives [45]

$$E_n = \frac{2}{n\pi hq^2 \sinh n\tau_c} \int_{-\pi}^{\pi} d\omega \cos n\omega \left(\frac{\partial\zeta}{\partial\tau}\right)_{\tau=\tau_c} \tag{10.100}$$

The functions $\zeta(\omega,\tau)$ and $\mathbf{u}(\omega,\tau)$ thus obtained represent the complete solution of the problem about the bilayer deformation. Below we proceed with the calculation of the force between two inclusions, which is due to the overlap of the deformed zones of the membrane around each inclusion.

10.4. LATERAL INTERACTION BETWEEN TWO IDENTICAL INCLUSIONS

10.4.1. DIRECT CALCULATION OF THE FORCE

The force approach (Section 7.1.5) can be applied to calculate the lateral capillary force, **F**, between two identical cylindrical inclusions, like those depicted in Figs. 10.1 and 10.6 [45]:

$$\mathbf{F} = 2\mathbf{U}_{\mathrm{II}} \cdot \oint_C dl \ \ (\mathbf{m}\cdot\underline{\boldsymbol{\sigma}}) \tag{10.101}$$

Here C denotes the contact line; the multiplier 2 accounts for the presence of two identical contact lines (upper and lower) on each inclusion. A difference between Eqs. (10.101) and (7.22) is that the membrane surface tension is a tensor, $\underline{\boldsymbol{\sigma}}$, rather than a scalar, see Eq. (10.68). Since the lateral stresses due to the deformation are zero, $\tau_{ij} = 0$, $(i, j = x, y)$, see Eqs. (10.54) and (10.63), in the present case there is no contribution analogous to $\mathbf{F}^{(kp)}$ in Eq. (7.23). In view of Eqs. (10.71) and (10.78), the two terms in Eq. (10.68) give rise to contributions, $\mathbf{F}^{(\sigma)}$ and

$\mathbf{F}^{(B)}$, originating from the scalar surface tension and bending moment, respectively; thus Eq. (10.101) can be represented in the form [45]:

$$\mathbf{F} = \mathbf{F}^{(\sigma)} + \mathbf{F}^{(B)} \tag{10.102}$$

$$\mathbf{F}^{(\sigma)} = 2\oint_C dl(\mathbf{U}_{\mathrm{II}} \cdot \mathbf{m})\sigma \tag{10.103}$$

$$\mathbf{F}^{(B)} = 2(k_c q^2 - B_0'/h) \oint_C dl(\mathbf{m} \cdot \nabla_s \zeta)(\mathbf{U}_{\mathrm{II}} \cdot \mathbf{n}) \tag{10.104}$$

As in Eq. (10.65), here ∇_s is a gradient operator in the curved surface $\zeta(x,y)$. The latter equations show that the interfacial bending moment can also give a contribution to the lateral capillary force: this conclusion has a more general validity, i.e. it holds for any interface, not only for lipid membranes. However, it is to be expected, that $\mathbf{F}^{(B)}$ can be comparable by magnitude with $\mathbf{F}^{(\sigma)}$ only for interfaces of low tension.

Geometrical considerations (see Fig. 10.6) yield

$$\mathbf{U}_{\mathrm{II}} \cdot \mathbf{m} = \tilde{\mathbf{n}} \cos\psi_c\,, \qquad \mathbf{U}_{\mathrm{II}} \cdot \mathbf{n} = \tilde{\mathbf{n}} \sin\psi_c \tag{10.105}$$

Note that the slope angle ψ_c varies along the contact line due to the overlap of the deformations created by the two inclusions. With the help of Eq. (10.66) one obtains

$$\cos\psi_c = \mathbf{e}_z \cdot \mathbf{n} = (1 + |\nabla_{\mathrm{II}}\zeta|^2)^{-1/2} \qquad \text{for } \tau = \tau_c \tag{10.106}$$

$$\sin\psi_c = \tilde{\mathbf{n}} \cdot \mathbf{n} = -(\tilde{\mathbf{n}} \cdot \nabla_{\mathrm{II}}\zeta)(1 + |\nabla_{\mathrm{II}}\zeta|^2)^{-1/2} = -\mathbf{m} \cdot \nabla_{\mathrm{s}}\zeta \qquad \text{for } \tau = \tau_c \tag{10.107}$$

Combining Eqs. (10.103)–(10.107) one derives [45]

$$\mathbf{F}^{(\sigma)} = 2\oint_C dl\ \tilde{\mathbf{n}}\ (1 + |\nabla_{\mathrm{II}}\zeta|^2)^{-1/2}\sigma \tag{10.108}$$

$$\mathbf{F}^{(B)} = 2(k_c q^2 - B_0'/h) \oint_C dl\ \tilde{\mathbf{n}}\ |\nabla_{\mathrm{II}}\zeta|^2\,(1 + |\nabla_{\mathrm{II}}\zeta|^2)^{-1} \tag{10.109}$$

Note that the surface tension σ in Eq. (10.108) can vary along the contact line; the dependence of σ on deformation can be derived from the tangential projection of the stress balance, Eq. (10.70). To do that we first note that the vectors of a covariant local basis in the upper bilayer surface can be expressed in the form [65]

$$\mathbf{a}_\nu = \mathbf{e}_\nu + \mathbf{e}_z\, \zeta_{,\nu} \qquad (\nu = 1, 2) \tag{10.110}$$

where $\mathbf{e}_1$ and $\mathbf{e}_2$ are the vectors of the local basis in the plane xy. Recalling that $p = 0$, with the help of Eqs. (10.54), (10.58), (10.66) and (10.110) one can derive [45]

$$\mathbf{n} \cdot \underline{\boldsymbol{\tau}} \cdot \mathbf{a}_\nu = (4\lambda/h)\zeta\, \zeta_{,\nu}\, (1 + |\nabla_{\mathrm{II}}\zeta|^2)^{-1/2} \tag{10.111}$$

Next, we substitute Eqs. (10.71), (10.73), (10.78) and (10.111) into the tangential balance, Eq. (10.70); as a result we obtain

$$\nabla_{\mathrm{II}}\sigma + (k_c q^2 - B_0'/h)(\mathbf{b}\cdot\nabla_{\mathrm{II}}\zeta) = (P_T - P_0)\,\nabla_{\mathrm{II}}\zeta + (2\lambda/h - \Pi')\nabla_{\mathrm{II}}\zeta^2 \tag{10.112}$$

where higher order terms have been neglected. One can employ Eq. (10.39) to derive: $\mathbf{b}\cdot\nabla_{\mathrm{II}}\zeta \approx (\nabla_{\mathrm{II}}\nabla_{\mathrm{II}}\zeta)\cdot\nabla_{\mathrm{II}}\zeta = \frac{1}{2}\nabla_{\mathrm{II}}|\nabla_{\mathrm{II}}\zeta|^2$. On substituting the last result in Eq. (10.112) and integrating one obtains the sought-for expression for the variation of the bilayer surface tension σ caused by the deformation [45]:

$$\sigma = \sigma_0 - \tfrac{1}{2}(k_c q^2 - B_0'/h)|\nabla_{\mathrm{II}}\zeta|^2 + (P_T - P_0)\zeta + (2\lambda/h - \Pi')\zeta^2 \tag{10.113}$$

Now we are ready to bring the expressions for $\mathbf{F}^{(\sigma)}$ and $\mathbf{F}^{(B)}$ in a form convenient for calculations. As we work with small deformations, we will keep only linear and quadratic terms with respect to ζ and its derivatives. We choose the x-axis to connect the two inclusions, as it is in Fig. 7.18; then $\mathbf{F}^{(\sigma)}$ and $\mathbf{F}^{(B)}$ have non-zero projection only along the x-axis, whose unit vector is denoted by $\mathbf{e}_x$. In addition, $\mathbf{e}_x \cdot \tilde{\mathbf{n}} = \cos\phi$, where ϕ is the azimuthal angle providing a parameterization of the contact line (see Fig. 7.20). Then from Eqs. (10.108), (10.109) and (10.113) we obtain [45]

$$F_x^{(\sigma)} \equiv \mathbf{e}_x \cdot \mathbf{F}^{(\sigma)} = -(\sigma_0 + k_c\, q^2 - B_0'/h)\; 2\oint_C dl\;\; |\nabla_{\mathrm{II}}\zeta|^2 \cos\phi \tag{10.114}$$

$$F_x^{(B)} \equiv \mathbf{e}_x \cdot \mathbf{F}^{(B)} = -(2\, B_0'/h\; - 2k_c\, q^2) \oint_C dl\;\; |\nabla_{\mathrm{II}}\zeta|^2 \cos\phi \tag{10.115}$$

It is convenient to introduce bipolar coordinates $(\omega,\ \tau)$ and to use the relationships

$$dl = \chi_c\, d\omega, \qquad \cos\phi = (\cosh\tau_c \cos\omega - 1)\chi_c/a, \qquad \nabla_{\mathrm{II}}\zeta\,\big|_{\tau=\tau_c} = \mathbf{e}_\tau \frac{1}{\chi_c}\left(\frac{\partial\zeta}{\partial\tau}\right)_{\tau=\tau_c} \tag{10.116}$$

where $\chi_c = a/(\cosh\tau_c - \cos\omega)$; cf. Eqs. (7.27) and (7.131). Finally, combining Eqs. (10.114) – (10.116) we obtain the non-zero x-component of the lateral capillary force between the two inclusions [45]:

$$F_x = F_x^{(\sigma)} + F_x^{(B)} = -\frac{2}{a}(\tilde{\sigma}_0 - k_c q^2)\int_0^{\pi} d\omega(\cosh\tau_c \cos\omega - 1)\left(\frac{\partial\zeta}{\partial\tau}\right)^2_{\tau=\tau_c} \tag{10.117}$$

where $\tilde{\sigma}_0 = \sigma_0 + B_0'/h$ has been introduced by Eq. (10.79). Note that the force F_x can be attractive or repulsive depending on whether $\tilde{\sigma}_0 > k_c q^2$ or $\tilde{\sigma}_0 < k_c q^2$. The respective interaction energy can be obtained by integration:

$$\Delta\Omega(L) = \int_L^{\infty} F_x(L) dL \tag{10.118}$$

As usual, L denotes the distance between the axes of the two cylindrical inclusions, see Fig. 10.1 and Eq. (10.97). To obtain numerical results one can first calculate the function $\zeta(\omega,\tau)$ as explained in Section 10.3.5, and then to substitute $(\partial\zeta/\partial\tau)_{\tau=\tau_c}$ in Eq. (10.117) to calculate F_x (and further $\Delta\Omega$) by means of numerical integration. Another (equivalent) approach, which yields directly expressions for calculating the interaction energy $\Delta\Omega$, is described in the next section.

10.4.2. THE ENERGY APPROACH

Mechanics and thermodynamics provide general expressions for the variation of the grand thermodynamic potential, $\delta\Omega$, rather than for Ω itself. One can find Ω by integrating $\delta\Omega$, however such an integration is straightforward only for uniform fluid phases [78,79] or isotropic elastic bodies [55].

In the case of curved interfaces $\delta\Omega$ depends on three independent variations: ζ, u_x and u_y, see e.g. Ref. [80], Eqs. (5.7)–(5.8) therein. In our case of a lipid bilayer, the solution of the mechanical problem for the hydrocarbon-chain interior, along with the boundary conditions at the bilayer surfaces, leads to connections between u_x, u_y and ζ. These connections enable one to obtain *a posteriori* an expression for Ω in terms of ζ only. As demonstrated in Ref. [45] as a

starting equation one can use the expression for the grand thermodynamic potential of a thin liquid film of surface tension σ and reference pressure of the film interior P_T, cf. Ref. [81]:

$$\Omega = 2\int_S ds\,\sigma - \int_{V_{\text{in}}} dV\,P_T - \int_{V_{\text{out}}} dV\,P_0 \tag{10.119}$$

Here S stands for the bilayer surface, and V_{in} and V_{out} denote, respectively, the volume of the bilayer interior and of the outer aqueous phase. Equation (10.119) expresses the grand thermodynamic potential for a *lipid bilayer* if σ is substituted from Eq. (10.113). The latter equation is nothing else than the integrated tangential stress balance at the bilayer surface, Eq. (10.70), in which the chain elasticity is involved through the elastic stress tensor $\underline{\boldsymbol{\tau}}$; see Eqs. (10.54) and (10.58). In other words, Eq. (10.113) contains in a "condensed" form the information about the bilayer mechanics for the "squeezing" mode of deformation. To demonstrate that we first transform the volume integrals:

$$\int_{V_{\text{in}}} dV\,P_T + \int_{V_{\text{out}}} dV\,P_0 = 2\int_{S_0} ds \left(\int_0^{h/2+\zeta} dz P_T + \int_{h/2+\zeta}^{z_1} dz P_0 \right) \tag{10.120}$$

where S_0 denotes the projection of the bilayer surface S on the bilayer midplane; in other words, S_0 is the whole xy-plane except the area excluded by the incorporated proteins; the exact position of the plane $z = z_1$ is not important because it does not affect the final result. In addition, using Eq. (10.113) we obtain

$$\int_S ds\,\sigma = \int_{S_0} ds\,(1+|\nabla_{\text{II}}\zeta|^2)^{1/2}[\sigma_0 - \tfrac{1}{2}(k_c q^2 - B_0'/h)|\nabla_{\text{II}}\zeta|^2 + (P_T - P_0)\zeta + (2\lambda/h - \Pi')\zeta^2] \tag{10.121}$$

The substitution of Eqs. (10.120) and (10.121) into Eq. (10.119), after some transformations, yields a relatively compact expression for the bilayer grand thermodynamic potential [45]:

$$\Omega = \int_{S_0} ds\,[(\tilde{\sigma}_0 - k_c q^2)\,|\nabla_{\text{II}}\zeta|^2 + 2(2\lambda/h - \Pi')\zeta^2] + \text{const.} \tag{10.122}$$

The validity of Eq. (10.122) can be confirmed by checking the correctness of its implications. First of all, imposing the requirement Ω to be minimum for any variations $\delta\zeta$ with *fixed* boundaries, from Eq. (10.122) one derives [45]:

$$\tilde{\sigma}_0\,\nabla_{\text{II}}^2\zeta - k_c q^2 \nabla_{\text{II}}^2\zeta = 2(2\lambda/h - \Pi')\zeta \tag{10.123}$$

The last equation is equivalent to Eq. (10.79) in view of Eq. (10.85). Moreover, in Ref. [45] it is proven that using the formula $F_x = -\delta\Omega/\delta L$ and variations at *movable* boundaries, from Eq. (10.122) one can deduce the expression for the lateral force, Eq. (10.117).

With the help of the identity $|\nabla_{\rm II}\zeta|^2 = \nabla_{\rm II}\cdot(\zeta\nabla_{\rm II}\zeta) - \zeta\,\nabla_{\rm II}^2\,\zeta$ and the Green integral theorem [69] Eq. (10.122) can be further transformed:

$$\Omega = 2(\widetilde{\sigma}_0 - k_c q^2)\oint_C dl\,(-\tilde{\mathbf{n}})\cdot(\zeta\nabla_{\rm II}\zeta) - \int_{S_0} ds\,[\,\widetilde{\sigma}_0\,\nabla_{\rm II}^2\,\zeta - k_c q^2\,\nabla_{\rm II}^2\,\zeta - 2(2\lambda/h - \Pi')\zeta]\zeta \qquad (10.124)$$

The multiplier 2 before the curvilinear integral comes from the two identical contours corresponding to the two inclusions. The integrand of the surface integral in Eq. (10.124) is zero owing to Eq. (10.123). Therefore, Eq. (10.124) can be presented in the simple form [45]

$$\Omega(L) = 4\pi(\widetilde{\sigma}_0 - k_c q^2) r_c\, h_c \tan\Psi_c(L) \qquad (10.125)$$

where

$$\tan\Psi_c(L) \equiv \frac{1}{2\pi r_c}\oint_C dl\,(-\tilde{\mathbf{n}}\cdot\nabla_{\rm II}\zeta) = \frac{1}{2\pi r_c}\int_{-\pi}^{\pi} d\omega\left(\frac{\partial\zeta}{\partial\tau}\right)_{\tau=\tau_c} \qquad (10.126)$$

expresses the average slope of bilayer surface at the contact line, cf. Fig. 10.6. Then the energy of interaction between the two inclusions can be written in the form

$$\Delta\Omega(L) \equiv \Omega(L) - \Omega(\infty) = 4\pi(\widetilde{\sigma}_0 - k_c q^2) r_c\, h_c\,[\tan\Psi_c(L) - \tan\Psi_c(\infty)] \qquad (10.127)$$

If the interfacial curvature effects are negligible ($B_0' = 0$, $k_c = 0$), then Eq. (10.127) reduces to Eq. (7.106) with an additional multiplier 2 accounting for the two contact lines per inclusion. The slope angle at infinite separation, $\Psi_c(\infty)$, can be identified with the angle ψ_c in Eq. (10.93). To determine $\Psi_c(L)$ one has to first calculate $\zeta(\omega,\tau)$ by numerical integration of Eq. (10.97), and then to carry out numerically the integration in Eq. (10.126). Alternatively, one can use the asymptotic formula

$$\tan\Psi_c(L) \approx q h_c\,\frac{\mathrm{K}_1(qr_c) - \frac{1}{2}qr_c\mathrm{K}_0(qL)}{\mathrm{K}_0(qr_c) + \mathrm{K}_0(qL)} \qquad (10.128)$$

which has been derived in Ref. [45] utilizing the method of reflections [82]. Substituting Eqs. (10.93) and (10.128) into Eq. (10.127) one obtains an asymptotic formula for $\Delta\Omega(L)$ [45]:

$$\Delta\Omega(L) = 4\pi(\tilde{\sigma}_0 - k_c q^2) q r_c h_c^2 \left[\frac{\mathrm{K}_1(qr_c) - \frac{1}{2} qr_c \mathrm{K}_0(qL)}{\mathrm{K}_0(qr_c) + \mathrm{K}_0(qL)} - \frac{\mathrm{K}_1(qr_c)}{\mathrm{K}_0(qr_c)} \right] \tag{10.129}$$

The numerical test of Eq. (10.129) shows that it gives $\Delta\Omega(L)$ with a good accuracy, see the next section.

10.5. NUMERICAL RESULTS FOR MEMBRANE PROTEINS

To illustrate the theoretical predictions in this section we present results from the numerical calculations [45] of the energy of interaction between two membrane proteins incorporated into a flat lipid bilayer. For this purpose parameters of the bacteriorhodopsin molecule, determined by means of electron microscopy [2,83], have been used: r_c = 1.5 nm and l_0 = 3.0 nm; see Fig. 10.6 for the notation. It is assumed that the hydrophobic α-helix regions of the bacteriorhodopsin molecule are imbedded inside the lipid bilayer. The following values of the *bilayer* mechanical parameters have been used: $\lambda = 2 \times 10^6$ N/m^2, σ_0 = 35 mN/m and $B_0' = -3.2 \times 10^{-11}$ N; with h = 3 nm one calculates $B_0'/h \approx -11$ mN/m, $\tilde{\sigma}_0 \equiv \sigma_0 + B_0'/h \approx 24$ mN/m and $q^{-1} \approx 3$ nm; in this case the term $k_c q^2 \approx 0.4$ mN/m is negligible compared to $\tilde{\sigma}_0$.

The mismatch between the height of the cylindrical inclusion, l_0, and the thickness of the non-disturbed layer, h, can be characterized by the quantity $h_c = (l_0 - h)/2$, see Fig. 10.6. In the experiments of Lewis and Engelman [30] l_0 was fixed, whereas h was varied by using lipids of various chain lengths. The respective experimental values of h have been used in our calculations: they are denoted on the respective curves in Figs. 10.7a,b, all of them corresponding to the same value of l_0 (to the same protein). The calculated curves of $\Delta\Omega/kT$ vs. $L/(2r_c)$ for $h_c > 0$ are shown in Fig. 10.7a, whereas those for $h_c < 0$ are shown in Fig. 10.7b. In general, one sees that the strength of the lateral capillary attraction increases with the increase of the magnitude of the mismatch, $|h_c|$. $\Delta\Omega$ can be larger than the thermal energy kT both for $h_c > 0$ and $h_c < 0$, except the cases with too small mismatch (h = 2.6 and 3.4 nm). For the curves with the largest mismatch, those with h = 1.55 nm in Fig. 10.7a and h = 3.75 nm in Fig. 10.7b, the calculated $\Delta\Omega$ (5–8 kT at close contact, $L = 2r_c$) is high enough to cause aggregation of the membrane protein molecules. Indeed, only in the latter two bilayers (h = 1.55 and 3.75 nm) did Lewis and Engelman [30] observe protein aggregation.

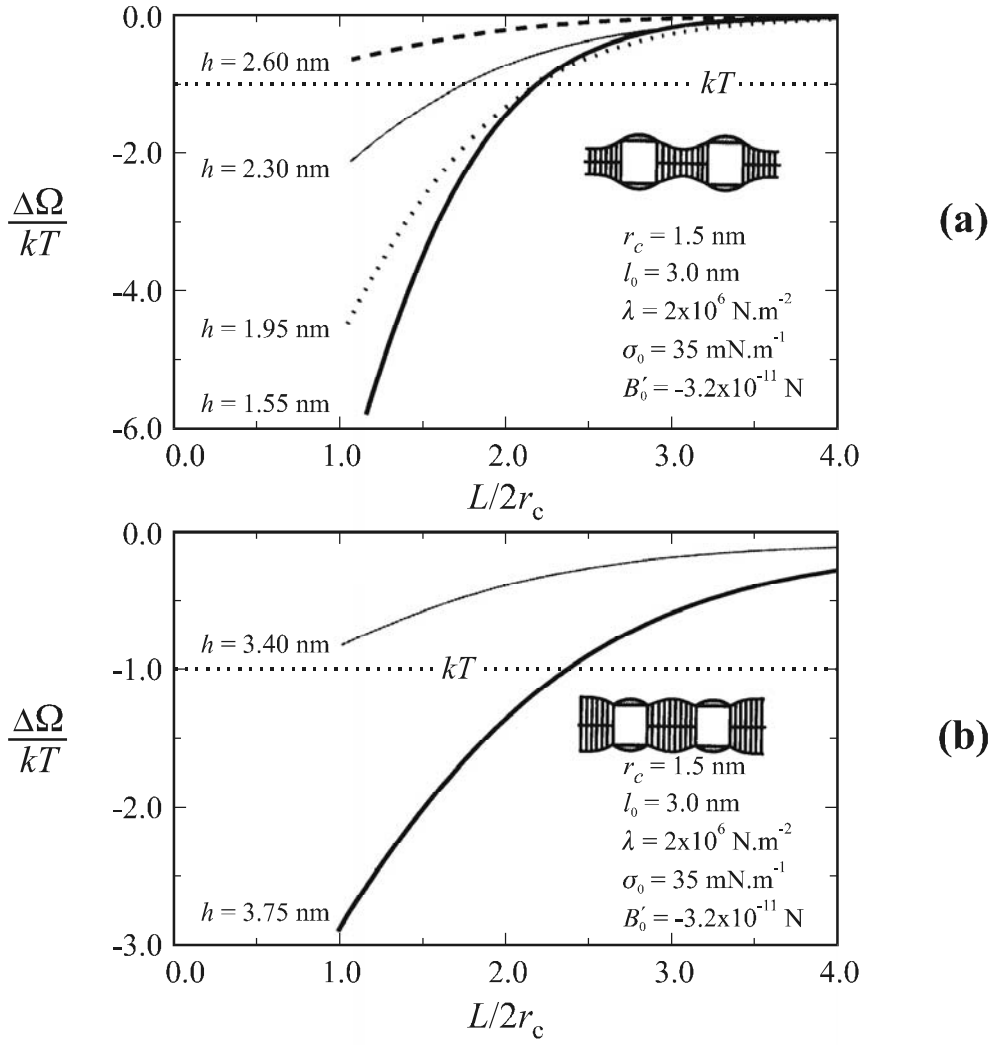

Fig. 10.7. Calculated in Ref. [45] interaction energy between two inclusions, $\Delta\Omega$, scaled by kT, vs. the separation L, scaled by r_c; the geometrical parameters of bacteriorhodopsin molecule taken from Refs. [2, 83] are $r_c = 1.5$ nm, $l_0 = 3.0$ nm; the values of h correspond to the experiments in Ref. [30]; (a) thinner bilayer, $h - l_0 < 0$; (b) thicker bilayer, $h - l_0 > 0$.

Comparing the curves with the same magnitude, but opposite signs of h_c ($h_c = 0.2$ for the curve with $h = 2.6$ nm in Fig. 10.7a, while $h_c = -0.2$ for the curve with $h = 3.4$ nm in Fig. 10.7b), one can conclude that $\Delta\Omega$ has larger magnitude and longer range in the case of $h_c < 0$, that is for a bilayer which is thicker than the inclusion, all other physical parameters being the same. This result is also consonant with the experimental observations of Lewis and Engelman [30]. Illustration of the same effect is given in Fig. 10.8, where it appears as a slight asymmetry of the $\Delta\Omega$ vs. h/l_0 curves with respect to the vertical line $h/l_0 = 1$. The curves in Fig. 10.8 are calculated for fixed distance, $L = 2r_c$, corresponding to close contact between the two

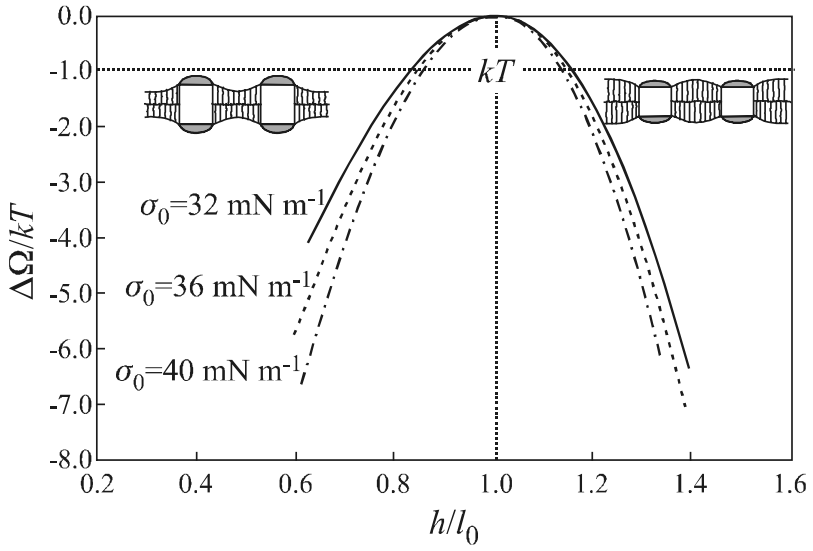

Fig. 10.8. Dimensionless interaction energy, $\Delta\Omega/kT$, vs. the dimensionless bilayer thickness, h/l_0, calculated in Ref. [45] for two bacteriorhodopsin molecules at close contact, $L = 2r_c$. The three curves correspond to three different values of the bilayer surface tension σ_0; the other parameters are as in Fig. 10.7.

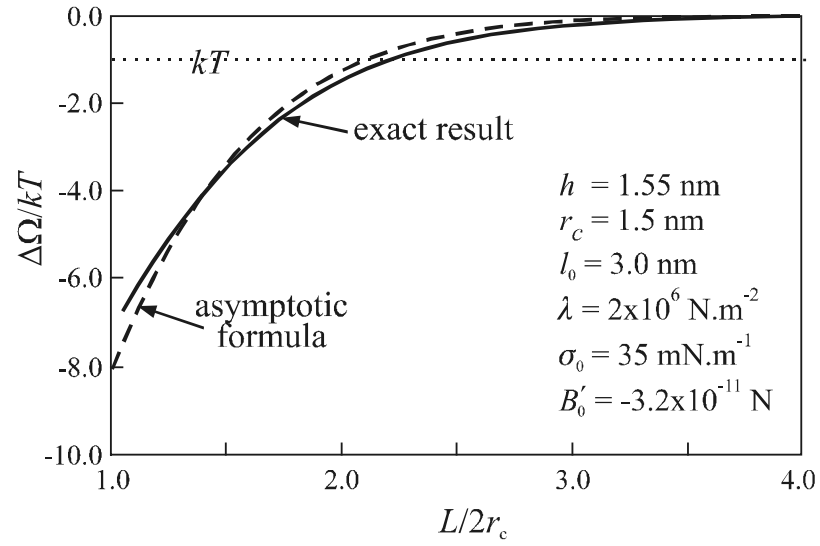

Fig. 10.9. Comparison of curves for $\Delta\Omega/kT$, vs. $L/2r_c$ calculated in Ref. [45] by means of Eq. (10.125) and the asymptotic Eq. (10.129); the bilayer thickness is $h = 1.55$ nm; the other parameters are as in Fig. 10.7.

membrane proteins. One sees in the figure that for small mismatches (around $h/l_0 = 1$) the energy of lateral attraction $\Delta\Omega$ is smaller than kT, i.e. negligible. However, $|\Delta\Omega|$ rises strongly when the mismatch increases in both directions. The increase of $|\Delta\Omega|$ with the rise of the surface tension of the non-perturbed bilayer, σ_0, is also illustrated in Fig. 10.8. We recall again

that σ_0 is a parameter of the "sandwich" model utilized here and it is to be distinguished from the total membrane tension, γ_b, which is usually rather low ($\gamma_b << 1$ mN/m). By definition (see Section 10.2.1) σ_0 is the interfacial tension of a lipid adsorption *monolayer* at oil-water interface for the same area per headgroup as in the bilayer. In the tension free state ($\gamma_b = 0$) the bilayer surface tension σ_0 is completely counterbalanced by the stresses in the hydrocarbon-chain region, see Eq. (10.8).

It should be noted that Figs. 10.7 and 10.8 give an illustration of the magnitude and range of the lateral protein-protein interaction energy, rather than a quantitative comparison between theory and experiment. An actual comparison demands to know the real values of the various parameters (λ, σ_0, etc.) which can depend on temperature and the nature of the lipid, the latter being different in the different experiments [30].

On the other hand, the comparison between the two versions of the theory, the *force* approach, Eqs. (10.117)–(10.118), and the *energy* approach, Eqs. (10.126)–(10.127), give coinciding numerical results for $\Delta\Omega$ as expected [45]. These equations have been used to calculate the curves in Figs. 10.7 and 10.8.

In Fig. 10.9 we compare plots of $\Delta\Omega$ vs. $L/2r_c$ calculated by means of the approximate Eq. (10.129) (the broken line) and by the more rigorous Eqs. (10.126)–(10.127) (the continuous line). This numerical text shows that the asymptotic formula (10.129) provides a good accuracy [45].

In Appendix 10A we describe the connections between the "sandwich" model presented in this chapter and the phenomenological model of a lipid membrane used by Dan et al. [38,40], which is based on a postulated expression for the free energy per molecule of a curved monolayer as a constituent part of bilayer lipid membrane.

10.6. SUMMARY

Although at body temperature a bilayer lipid membrane behaves as a two-dimensional liquid, mechanically it cannot be simply described as a thin liquid film. The reason is that the hydrocarbon-chain interior of the membrane exhibits elastic behavior if the thickness of the bilayer is varied. This hybrid behavior of the lipid bilayers (neither liquid nor solid) can be

described by means of a mechanical model, which treats the membrane as a special elastic film (the hydrocarbon chain interior) sandwiched between two Gibbs dividing surfaces (accounting for the polar headgroup regions on the membrane surfaces). The latter *"sandwich" model* involves mechanical parameters such as the shear elastic modulus of the hydrocarbon chain interior λ, and the properties of the two bilayer surfaces: surface tension σ, stretching (Gibbs) elasticity E_G, surface bending moment B_0 (proportional to the spontaneous curvature), surface bending and torsion elastic moduli, k_c and $\bar{k}_c$. All these parameters can be determined in experiments with lipid monolayers and bilayers. In the framework of the "sandwich" model the *tension-free state* of a bilayer is attributed to the counterbalancing of compressing stresses in the membrane surfaces by stretching stresses in the membrane interior, see Eq. (10.7). A mechanical analysis of the bilayer deformations enables one to derive expressions for the total stretching, bending and torsion moduli of the membrane as a whole, K_s, k_t and $\bar{k}_t$, in terms of the aforementioned mechanical parameters of the model, see Eqs. (10.21), (10.49) and (10.50).

Inclusions (like proteins) in a lipid membrane cause deformations in its surfaces accompanied by displacements in the membrane hydrocarbon interior, see Figs. 10.1 and 10.6. The resulting stresses are described by an appropriate constitutive relation, Eq. (10.54), and the interfacial stress balance, Eq. (10.65). The model provides a set of differential equations for determining the displacement vector, **u**, and the interfacial shape, $z = \zeta(x,y)$. The linearized problem can be reduced to solving a fourth-order differential equation for $\zeta(x,y)$, Eq. (10.79). The latter could have monotonic and oscillatory solutions for the membrane profile depending on the values of the involved physical parameters. The case of monotonic solutions (corresponding to not-too-low membrane surface tension) is investigated in details; in this case the shape of the membrane surfaces is governed by a second order differential equation, Eq. (10.85), which is analogous to the Laplace equation of capillarity. The account for the compressing stresses at the bilayer surfaces and the elastic stresses in the bilayer interior leads to the appearance of the bilayer surface tension σ_0 and the chain shear elasticity λ in the expression for the characteristic capillary length q^{-1}, see Eq. (10.84).

The theory of the capillary immersion forces, presented in Chapter 7, can be extended and applied to describe the interactions between two inclusions in a lipid membrane; the derived expressions for the interaction force and energy are Eqs. (10.117) and (10.125). The range of

the resulting attractive interaction turns out to be of the order of several inclusion radii. The magnitude of the interaction energy $\Delta\Omega$ is proportional to the mismatch h_c between the hydrophobic zone of the inclusion and the hydrocarbon core of the bilayer. For not-too-small h_c the magnitude of $\Delta\Omega$ can be from 2 to 8 kT at close contact of the inclusions (Figs. 10.7–10.9); this is sufficient to bring about their aggregation.

An asymptotic formula for $\Delta\Omega$ is derived, Eq. (10.129), which compares well with the numerical calculations; this formula makes the calculation of the interaction energy much easier at the cost of some approximations. The theoretical predictions qualitatively agree with the experimental observations of Lewis and Engelman [30], although more reliable data for the membrane mechanical parameters are needed to achieve a real quantitative comparison between theory and experiment. The parameters of the "sandwich" model can be related to the parameters of the phenomenological model by Dan et al. [38], which is also designed to describe the interactions between inclusions in lipid membranes, see Appendix 10A.

The presented mechanical model of lipid membranes can be helpful for the theoretical description of various processes involving bilayer deformations and for the interpretation of experimental data about the interactions and aggregation of protein inclusions.

10.7. REFERENCES

1. J.D. Robertson J. Cell. Biol. 19 (1963) 201.
2. R. Henderson, P.N.T. Unwin, Nature 257 (1975) 28.
3. P.N.T. Unwin, G. Zampighi, Nature 283 (1980) 545.
4. A.K. Mitra, M.P. McCarthy, R.M. Stroud, J. Cell Biol. 109 (1989) 755.
5. R. Henderson, J.M. Baldwin, T.A. Ceska, F. Zemlin, E. Beckmann, K.H. Downing, J. Mol. Biol. 213 (1990) 899.
6. T. Gil, J.H. Ipsen, O.G. Mouritsen, M.C. Sabra, M.M. Sperotto, M. Zuckermann, in BBA Reviews on Biomembranes, Vol. 1376 (3), Elsevier, Amsterdam, 1998; pp. 245-266.
7. R. Lipowsky, E. Sackmann (Eds.), in: Handbook of Biological Physics, Vol. 1A&B. Elsevier, Amsterdam, 1995; pp. 1–1020.
8. O.G. Mouritsen, Curr. Opin. Coll. Interface Sci. 3 (1998) 78.
9. S. Marčelja, Biochim. Biophys. Acta 367 (1974) 165.

10. D.W.R. Gruen, Biochim. Biophys. Acta 595 (1980) 161.
11. A.G. Petrov, I. Bivas, Prog. Surface Sci. 16 (1984) 389.
12. A. Ben-Shaul, W.M. Gelbart, Ann. Rev. Phys. Chem. 36 (1985) 179.
13. I. Szleifer, D. Kramer, A. Ben-Shaul, W.M. Gelbart, S.A. Safran, J. Chem. Phys. 92 (1990) 6800.
14. M. Kléman, Proc. Roy. Soc. London A, 347 (1976) 387.
15. E. Evans, R. Skalak, Mechanics and Thermodynamics of Biomembranes, CRC Press, Boca Raton, 1980.
16. A.G. Petrov, M.D. Mitov, A. Derzhanski, in: Advances in Liquid Crystal Research and Application, Pergamon, Oxford, Academia Kiado, Budapest, 1980; p. 695.
17. H.W. Huang, Biophys. J. 50 (1986) 1061.
18. P. Helfrich, W. Jakobson, Biophys. J. 57 (1990) 1075.
19. H. Schröder, J. Chem. Phys. 67 (1977) 1617.
20. J.C. Owicki, M.W. Springgate, H.M. McConnell, Proc. Natl. Acad. Sci. USA 75 (1978) 1616.
21. J.C. Owicki, H.M. McConnell, Proc. Natl. Acad. Sci. USA 76 (1979) 4750.
22. P. Joost, O.H. Grifith, R.A. Capaldi, G. Vanderkooi, Biochim. Biophys. Acta 311 (1973) 141.
23. J.H. Davis, D.M. Clare, R.S. Hodges, M. Bloom, Biochemistry 22 (1983) 5298.
24. M. Esmann, A. Watts, D. Marsh, Biochemistry 24 (1985) 1386.
25. E. Favre, A. Baroin, A. Bienvenue, P.F. Devaux, Biochemistry 18 (1979) 1156.
26. G. Benga, R.P. Holmes, Prog. Biophys. Molec. Biol. 43 (1984) 195.
27. M. Bloom, E. Evans, O.G. Mouritsen, Quart. Rev. Biophys. 24 (1991) 293.
28. Y.S. Chen, W.L. Hubbel, Exp. Eye Res. 17 (1973) 517.
29. J. Davoust, A. Bienvenue, P. Fellmann, P.F. Devaux, Biochim. Biophys. Acta 596 (1980) 28.
30. B.A. Lewis, D.M. Engelman, J. Mol. Biol. 166 (1983) 203.
31. J.C. Huschilt, R.S. Hodges, J.H. Davis, Biochemistry 24 (1985) 1377.
32. J. Riegler, H. Möhwald, Biophys. J. 49 (1986) 1111.
33. J. Peschke, J. Riegler, H. Möhwald, Eur. Biophys. J. 14 (1987) 385.
34. M.Ge, J.H. Freed, Biophys. J. 76 (1999) 264.
35. O.G. Mouritsen, M. Bloom, Biophys. J. 46 (1984) 141.

36. M.M. Sperotto, O.G. Mouritsen, Eur. Biophys. J. 19 (1991) 157.
37. M. Goulian, R. Bruinsma, P. Pincus, Europhys. Lett. 22 (1993) 145.
38. N. Dan, P. Pincus, S.A. Safran, Langmuir 9 (1993) 2768.
39. N. Dan, A. Berman, P. Pincus, S.A. Safran, J. Phys. II France 4 (1994) 1713.
40. H. Aranda-Espinosa, A. Berman, N. Dan, P. Pincus, S.A. Safran, Biophys. J. 71 (1996) 648.
41. N. Dan, S.A. Safran, Biophys. J. 75 (1998) 1410.
42. J.N. Israelachvili, Biochim. Biophys. Acta, 469 (1977) 221.
43. P. Sens, M.S. Turner, P. Pincus, Phys. Rev. E, 55 (1997) 4394.
44. R.S. Cantor, J. Phys. Chem. B 101 (1997) 1723.
45. P.A. Kralchevsky, V.N. Paunov, N.D. Denkov, K. Nagayama, J. Chem. Soc. Faraday Trans. 91 (1995) 3415.
46. L. Shen, D. Bassolino, T. Stouch, Biophys. J. 73 (1997) 3.
47. S.J. Bussell, D.L. Koch, D.A. Hammer, J. Fluid. Mech. 243 (1992) 679.
48. B.V. Derjaguin, E.V. Obuhov, Nature (London) 138 (1936) 330.
49. B.V. Derjaguin, N.V. Churaev, V.M. Muller, Surface Forces, Plenum Press, New York, 1987.
50. J.N. Israelachvili, Intermolecular and Surface Forces, Academic Press, New York, 1992.
51. I.B. Ivanov, P.A. Kralchevsky, Mechanics and Thermodynamics of Curved Thin Films, in: I.B. Ivanov (Ed.) Thin Liquid Films, M. Dekker, New York, 1988; p. 49.
52. S. Nir, C.S. Vassilieff, Van der Waals Interactions in Thin Films, in: I.B. Ivanov (Ed.) Thin Liquid Films, M. Dekker, New York, 1988; p. 207.
53. A.I. Rusanov, Phase Equilibria and Surface Phenomena, Khimia, Leningrad, 1967 (in Russian); Phasengleichgewichte und Grenzflächenerscheinungen, Akademie Verlag, Berlin, 1978.
54. B.Y. Yue, C.M. Jackson, J.A.G. Taylor, J. Mingins, B.A. Pethica, J. Chem. Soc. Faraday Trans. I, 72 (1976) 2685.
55. L.D. Landau, E.M. Lifshitz, Theory of Elasticity, Pergamon Press, Oxford, 1970.
56. L. Fernandez-Puente, I. Bivas, M.D. Mitov, P. Méléard, Europhys. Lett. 28 (1994) 181.
57. E. Evans, Adv. Colloid Interface Sci. 39 (1992) 103.
58. W. Helfrich, R.-M. Servuss, Nuovo Cimento D3 (1984) 137.
59. W. Helfrich, Z. Naturforsch. 28C (1973) 693.

60. A.E.H. Love, A Treatise of the Mathematical Theory of Elasticity, University Press, Cambridge, 1927.

61. J. Ennis, J. Chem. Phys. 97 (1992) 663.

62. P.A. Kralchevsky, T.D. Gurkov, K. Nagayama, J. Colloid Interface Sci. 180 (1996) 619.

63. J. Mingins, D. Stigter, K.A. Dill, Biophys. J. 61 (1992) 1603.

64. J.G.H. Joosten, Light Scattering from Thin Liquid Films, in: I.B. Ivanov (Ed.) Thin Liquid Films, M. Dekker, New York, 1988; p. 569.

65. P.A. Kralchevsky, I.B. Ivanov, J. Colloid Interface Sci. 137 (1990) 234.

66. P.M. Naghdi, in: Handbuch der Physik, Vol. Via/2, Springer, Berlin, 1972.

67. Y.S. Podstrigach, Y.Z. Povstenko, Introduction in Mechanics of Surface Phenomena in Deformable Solids, Naukova Dumka, Kiev, 1985 (in Russian).

68. C.E. Weatherburn, Differential Geometry of Three Dimensions, Cambridge Univ. Press, Cambridge, 1930.

69. A.J. McConnell, Application of Tensor Analysis, Dover, New York, 1957.

70. P.A. Kralchevsky, J.C. Eriksson, S. Ljunggren, Adv. Colloid Interface Sci. 49 (1994) 19.

71. S. Ljunggren, J.C. Eriksson, P.A. Kralchevsky, J. Colloid Interface Sci. 191 (1997) 424.

72. J. Meunier, L.T. Lee, Langmuir 7 (1991) 1855.

73. E. Janke, F. Emde, F. Lösch, Tables of Higher Functions, McGraw-Hill, New York, 1960.

74. M. Abramowitz, I.A. Stegun, Handbook of Mathematical Functions, Dover, New York, 1965.

75. G.A. Korn, T.M. Korn, Mathematical Handbook, McGraw-Hill, New York, 1968.

76. A. Constantinides, Applied Numerical Methods with Personal Computers, McGraw-Hill, New York, 1987.

77. R.W. Hockney, J.W. Eastwood, Computer Simulation Using Particles, McGraw-Hill, New York, 1981.

78. J.W. Gibbs, The Scientific Papers of J.W. Gibbs, Vol.1, Dover, New York, 1961.

79. S. Ono, S. Kondo, Molecular Theory of Surface Tension in Liquids, in: S. Flügge (Ed.), Handbuch der Physik, vol. 10, Springer, Berlin, 1960, p. 134.

80. P.A. Kralchevsky, J. Colloid Interface Sci. 137 (1990) 217.

81. P.A. Kralchevsky, K. Nagayama, Langmuir 10 (1994) 23.

82. J. Happel, H. Brenner, Low Reynolds Number Hydrodynamics, Prentice Hall, New York, 1965; Martinus Nijhoff, Hague, 1983.

83. P.N.T. Unwin, R. Henderson, J. Mol. Biol. 94 (1975) 425.